

Synthetic Air Data System

F. Adhika Pradipta Lie* and Demoz Gebre-Egziabher†
 University of Minnesota, Twin Cities, Minneapolis, Minnesota 55455

DOI: 10.2514/1.C032177

A method for estimating the airspeed, angle of attack, and sideslip without using a conventional, pitot-static air data system is presented. The method relies on measurements from Global Positioning System, an inertial measurement unit, and a low-fidelity model of the aircraft's dynamics, which are fused using two cascaded extended Kalman filters. In the cascaded architecture, the first filter uses information from the inertial measurement unit and Global Positioning System to estimate the aircraft's absolute velocity and attitude. These estimates are used as the measurement updates for the second filter in which they are fused with the aircraft dynamics model to generate estimates of the airspeed, angle of attack and sideslip. Methods for dealing with the time and interstate correlation in the measurements coming from the first filter are discussed. Simulation and flight-test results of the method are presented. Simulation results show that the root mean square error of the airspeed estimate is less than 1 m/s. The nominal errors from the flight test on airspeed, angle of attack, and sideslip are less than 2.5 m/s, 2 deg, and 1 deg, respectively. Factors that affect the accuracy, including the implication and impact of using a low-fidelity aircraft model, are discussed.

Nomenclature	
a	= acceleration vector
b, \bar{c}, S	= wingspan, mean aerodynamic chord length, and wing reference area
$b_a(\cdot), b_g(\cdot)$	= accelerometer (a) and gyro (g) bias on (\cdot) axis
b_D, b_ϕ, b_θ	= correlated error states
b_ψ	
C_D	= drag coefficient
C_L	= lift coefficient
C_l	= rolling moment coefficient
C_m	= pitching moment coefficient
C_n	= yawing moment coefficient
C_N^B	= direction cosine matrix from North-East-Down frame to body frame
C_P	= coefficient of power
C_T	= coefficient of thrust
C_Y	= side force coefficient
d	= propeller diameter
$E[\cdot]$	= expectation operator
F	= Jacobian matrix
f	= propeller rotational speed, Hz
f^x, f^y, f^z	= accelerometer output on x , y , and z axes
G	= shaping matrix
g	= acceleration due to gravity
H	= observation matrix
J	= advance ratio, $\frac{V}{f d}$
K	= Kalman gain
$m, I_{(\cdot)}$	= aircraft's mass and rotational inertia about (\cdot) axis
NED	= North-East-Down coordinate frame
$n_{(\cdot)}, \sigma_{(\cdot)}$	= white noise in (\cdot) channel and its standard deviation
P	= state error covariance matrix
p, q, r	= body (pitch, roll, and yaw) rates
Q	= process noise covariance matrix
R	= measurement noise covariance matrix
r_x, r_y, r_z	= three-dimensional position vector of the thrust point with respect to aircraft center of gravity
T, \mathcal{T}	= propulsive thrust and propeller torque exerted on the aircraft
V	= airspeed magnitude
V_{EB}^N	= ground speed resolved on North-East-Down frame, $[V_N \ V_E \ V_D]^T$
V_{WB}^B	= airspeed resolved on body frame, $[u \ v \ w]^T$
$\tilde{\mathbf{W}}$	= two-dimensional wind field in the north and east directions, $[\tilde{W}_N \ \tilde{W}_E \ 0]^T$
W_N, W_E	= pseudowind estimate in the north and east directions
\mathbf{x}	= state vector
X, Y, Z	= summation of aerodynamic and propulsive forces resolved in the body frame
\mathbf{y}	= measurement vector
α, β	= angle of attack and sideslip angle
$\delta(\cdot)$	= Kronecker delta function
$\delta_e, \delta_a, \delta_r$	= elevator, aileron, and rudder deflections
ρ	= air density
$\tau_{(\cdot)}$	= correlation time constant of a first-order Gauss-Markov process
Φ	= state transition matrix
ϕ, θ, ψ	= pitch, roll, and yaw angles
$\omega^x, \omega^y, \omega^z$	= rate gyro output on x , y , and z axes
(\cdot)	= estimate of (\cdot)
$(\cdot)_k$	= quantity (\cdot) at time k
$(\cdot)^-$	= estimate of (\cdot) before measurement update
$(\cdot)^+$	= estimate of (\cdot) after measurement update

Presented as Paper 2012-4704 at the AIAA Guidance, Navigation, and Control Conference and Exhibit, Minneapolis, MN, 13–16 August 2012; received 23 October 2012; revision received 20 December 2012; accepted for publication 21 December 2012; published online 30 May 2013. Copyright © 2013 by F. Adhika Pradipta Lie and Demoz Gebre-Egziabher. Published by the American Institute of Aeronautics and Astronautics, Inc., with permission. Copies of this paper may be made for personal or internal use, on condition that the copier pay the \$10.00 per-copy fee to the Copyright Clearance Center, Inc., 222 Rosewood Drive, Danvers, MA 01923; include the code 1542-3868/13 and \$10.00 in correspondence with the CCC.

*Research Assistant, Department of Aerospace Engineering and Mechanics; adhika@aem.umn.edu. Student Member AIAA.

†Associate Professor, Department of Aerospace Engineering and Mechanics; gebre@aem.umn.edu. Member AIAA.

I. Introduction

THE performance of an airplane in flight depends, in part, on the magnitude of its velocity relative to the air mass in which it is flying. It also depends on the orientation of the airplane relative to this velocity vector. The speed and orientation of the airplane relative to the air mass are quantified by three parameters: airspeed, V ; angle of attack, α ; and sideslip angle, β . An accurate estimate of these parameters is key to the efficient and safe operation of aircraft regardless of whether they are being operated by a human pilot or an automatic control system. For example, the airspeed is used to define the minimum speed for safe operation (stall speed) and the maximum speed beyond which aircraft structural damage can occur. Angle of

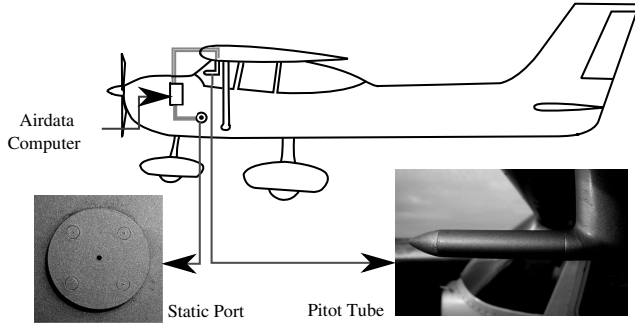


Fig. 1 Pitot-static system.

attack and sideslip measurements are used to ensure an airplane does not operate in a region from which recovery from a flight upset is not possible.

Traditionally, these quantities are determined by an air data system that consists of a pitot-static subsystem and angle of attack vanes, which provide measurements to a central air data computer. The airspeed is determined from measurements made by a pitot-static system. The pitot-static system consists of pressure sensors and specialized piping arranged as shown schematically in Fig. 1. Most angle of attack sensors are in the form of a mechanical vane that aligns with the local airflow, like the one shown in Fig. 2a, or a multiport pitot tube that estimates the angle of attack from differential pressure, like the one shown in Fig. 2b. Sideslip measurements can also be made using this multiport pitot tube. Because an accurate measurement of the airspeed is critical to safe operation, it is not uncommon to find doubly redundant airspeed, angle of attack, and sideslip (such as [1][‡]) measurement systems installed on an airplane.

A. Motivation

The recent interest in small, uninhabited aerial vehicles (UAVs) and the potential of operating them in the national airspace system have given rise to an interest in how to design low-cost and highly reliable avionics. This is motivated by the need to develop avionics that meet the size, weight, and power (SWAP) constraints of UAVs. For example, the use of triply redundant avionics is not always possible in these small vehicles, and so the idea of analytical redundancy has received some attention. Analytical redundancy is a term used to describe the idea of replacing the physical hardware with analytical models in multiple-redundant safety-critical systems [2]. A low-cost device or method capable of making reliable estimates of these three air data quantities, namely, V , α , and β , is highly desirable in its own right. Not only is it useful for SWAP-constrained applications such as an unmanned aerial system, but it is also very attractive for cost-sensitive applications such as general aviation.

The enablers of a low-cost solution to air data estimation are inexpensive sensors and powerful computers that allow real-time sensor fusion. The result of this is a statistical blending of information from different sensors to generate optimum unbiased estimates of the desired quantities. This paper uses this technique to provide a low-cost synthetic estimate of V , α , and β from an inertial measurement unit (IMU) and a Global Positioning System (GPS) receiver. The independence of this system from the conventional air data system allows a great number of potential applications. For example, aside from providing a backup to the primary air data computers, this synthetic estimate can also enhance fault detection and isolation in the event of a failure in the primary or traditional air data system.

B. Prior Art

The idea of synthetic air data systems is not new, and algorithms for generating estimates of V , α , and β using nontraditional sensors are described in the open literature. Most of these works [3–6] treat the triplet V , α , and β separately. They assume the availability of

independent airspeed measurement and an accurate lift coefficient, C_L , model to estimate α and β using IMU measurements. The accuracy of α and β estimates depends largely on the fidelity of the C_L model and the quality of the inertial sensor used.

Because of the limited computational power at that time, Zeis [3] devised an approach that breaks the problem into two and uses two separate estimators: one to estimate α in real time (in-flight estimator) and another for postflight estimation of both α and β . The online estimator generates a snapshot estimate of α from a model of C_L for the aircraft. The load factor $n = \frac{L}{mg}$ computed from a vertical accelerometer with attitude and gravity compensation and rate gyro measurements are used to replace the complex model of the wing and horizontal stabilizer interaction in generating lift. The equation relating C_L to α is at the heart of this estimator and has the following mathematical form [3]:

$$C_L = \frac{n \cdot mg \cdot x_t + \dot{q}I_y + pr(I_x - I_z) - C_{m_0}(1/2)\rho V^2 S \bar{c}}{\frac{1}{2}\rho V^2 S x_t [1 + (x_{wb}/x_t)]} \quad (1)$$

where x_{wb} is the distance between the center of gravity of the aircraft and the wing-body aerodynamic center, and x_t is the distance between the center of gravity of the aircraft and the aerodynamic center of the horizontal stabilizer. The function $Fn(\cdot)$ that relates C_L to α can be empirical and determined by curve fitting the available aerodynamic data. With the navigation-grade inertial navigation system (INS) installed on the F-15 and the available C_L vs α relationship, this in-flight estimator was reported to generally satisfy the 0.5 deg accuracy requirement on α . Further, an accurate knowledge of C_{m_0} was found to be a critical factor to accurately estimate α .

The postflight estimator uses linearized aircraft dynamics in a Kalman filter to estimate α and β using attitude and rate gyro measurements from an IMU. However, the limited computational power that was available at the time (late 1980s) precluded the use of this type of estimator in flight, especially when the flight and trim conditions were changing. No comment was made with regards to use of this estimator with real flight data. Simulated data showed 0.25 deg accuracy in estimating α and β .

Although this method of estimating α seems to work very well, its reliance on a navigation-grade IMU (as defined in Groves [7]) makes it prohibitively expensive for low-cost applications. A low-cost system will use inertial sensors that are in the category identified by the moniker automotive/consumer grade [8]. Inertial sensors of this quality have large, time-varying output errors. When these sensors are used to mechanize an INS, the time-varying output errors (accelerometer and rate gyro biases) must be estimated continuously and compensated. Otherwise, the load factor estimates will be inaccurate due to drifting attitude used to separate the effect of mechanical acceleration and gravity. Another drawback to this method is that it is not completely synthetic. That is, it requires a pitot measurement to provide an airspeed estimate.

A similar approach was taken by NASA Langley Research Center [6] to develop an angle of attack command augmentation system for the AirSTAR flight-test facility. Although this approach showed success in estimating angle of attack in real time, this method relies on the presence of a pitot-static system to take airspeed out of the equations. Moreover, the process is algebraic and does not take into account the stochastic nature of the sensor measurement errors.

Researchers at the Institute of Flight Mechanics and Flight Control at Technische Universität München [4,5] synthesized an integrated air data and navigation system using low-cost commercial off-the-shelf sensors: a Micro Electronic Mechanical System (MEMS) IMU, a single-frequency GPS receiver, and an airspeed sensor in the form of a pitot/static system. The angle of attack and sideslip angle are determined using inertial sensor outputs and an aerodynamic coefficient model. An aerodynamic angle of attack is calculated using an approach similar to Eq. (1). It is then combined with the kinematic angle of attack, α_K , using a complimentary filter to increase the system's bandwidth:

[‡]Data available online at <http://www.flightglobal.com/news/articles/flight-test-airbus-a380-209189/> [retrieved 13 March 2013].

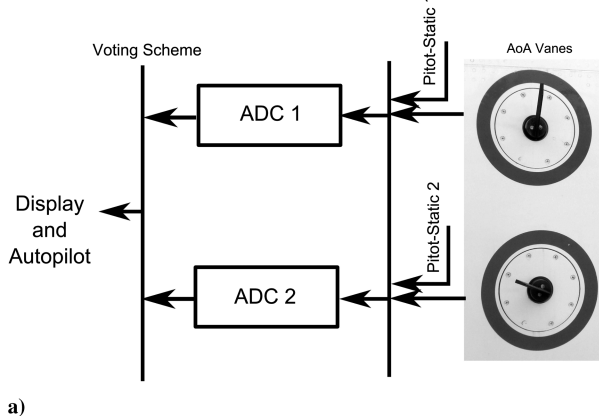


Fig. 2 Angle of attack sensors: a) vane type on Airbus 330 and b) five-hole pitot probe on F-16A.

$$\alpha_K = \frac{\theta - \tan^{-1} \left(\frac{-V_D}{\sqrt{V_N^2 + V_E^2}} \right)}{\cos \phi} \quad (2)$$

A complementary filter essentially puts a low-pass filter on the aerodynamic angle of attack and a high-pass filter on the kinematic angle of attack, α_K , to enhance the filter performance across the frequency of interest.

Colgren et al. [9–11] presented a series of papers on using inertial sensors to estimate the angle of attack and sideslip angle. To estimate aerodynamic angles, gust compensation must be made. This calls for the aerodynamic model of the aircraft to subtract the dynamic acceleration from the total acceleration as measured by an accelerometer. These works culminated in a U.S. patent in 2001 [12].

Wise [13] put air data estimation into a filtering framework. An extended Kalman filter (EKF) was devised to estimate the angle of attack and sideslip angle from INS-derived pitch and roll angles and IMU outputs (rotation rates and specific forces). The aircraft dynamics model was used in the filter time update. Dynamic pressure measurement from a pitot-static system was used in calculating the aircraft response, although the airspeed V is also part of the state vector. This work also culminated in a U.S. patent in 2005 [14].

Recent advances of navigation technology have enabled ground speed measurements to be made at a very low cost. However, ground speed is the algebraic sum of the velocity of the aircraft relative to the surrounding air mass (airspeed) and the velocity of the surrounding air mass relative to the ground (wind speed). Hence, to estimate α and β without the availability of the direct measurement of airspeed, wind estimation is an integral part of the problem. Although there is prior work in wind estimation (e.g., [15–17]), these approaches require the presence of a pitot-static system.

C. Contribution

This paper describes a method of estimating the triplet V , α , and β using an automotive-grade IMU without relying on a pitot measurement. More specifically, it combines information from IMU, GPS, and aircraft dynamics to estimate the airspeed, angle of attack, and sideslip without the use of a pitot-static system or angle of attack/sideslip vanes. The approach presented uses a federated EKF architecture in which two estimators are cascaded in series. Although this approach is not intuitive at first, the analysis presented in this paper shows its necessity especially when low-cost inertial sensors are used. The output of the first estimator is used as an input to the second estimator. The second estimator fuses the information from the first filter with information derived from a low-fidelity aircraft dynamic model to extract the states of interest, namely, V , α , and β . The filter architecture presented in this paper systematically handles the issue of time-correlated measurement, which is often neglected when cascading two estimators in series. The main output of the cascaded estimators are the six navigation states (position, velocity, and attitude) and three air data quantities (V , α , and β). In addition to

these quantities, the filter also estimates inertial sensor biases and six other states that account for the time correlation in the measurements that come into the second filter. The first two of these states include the estimate of the two-dimensional (2-D) wind field. These two states are termed pseudowind estimates because they include both the estimate of the wind field and the time correlation between successive measurements. Finally, the filter provides a metric of the quality of the estimates in the form of a covariance matrix. The work reported here is an extension and elaboration of work initially reported in [18].

D. Paper Organization

The remainder of this paper is organized as follows. Section II provides a detailed description of the filter architecture used in this work. Several alternatives to the architecture used in this work are provided in Sec. II.B. Section II.B presents the nonlinear six-degree-of-freedom (DOF) rigid-body aircraft model used in this filter, and Secs. II.C and II.D outline the details of the EKF mechanization. Section IV presents the performance analysis result of the synthetic air data system using simulated data obtained from a flight simulator. In Sec. V, flight-test results are used to show how the performance of the synthetic air data system compares against the traditional air data system.

II. System Architecture

In theory, it is not difficult to generate a synthetic estimate (i.e. without using conventional pitot-static system) of the V , α , and β triplet by fusing the outputs from an INS with information about wind speed. The INS generates an estimate of the absolute velocity (or ground speed) of the airplane. A vector subtraction of the wind speed velocity from the absolute velocity will yield airspeed. In practice, however, this presents two challenges. First, it is difficult (if not impossible) to obtain measurements of the wind speed for each and every point in space in which an airplane will fly. Even if wind speed measurements at discrete points in space (a grid, for example) were available, models for extrapolating wind speed to arbitrary points in space [19–21] may not be sufficiently accurate to allow generating usable estimates of the V , α , and β triplet. Second, the synthetic estimates of V , α , and β rapidly become unusable as the inertial sensor quality degrades. An alternate approach is to use an estimator to combine estimates of ground speed and attitude from a navigation system (such as an integrated INS/GPS system) with estimates of airspeed and attitude derived from a kinetic (dynamic) model of the aircraft. The airspeed estimate generated from the dynamic model of the aircraft alone would be not be very accurate; small errors in the dynamic model would lead to large uncertainties in the airspeed estimate. However, by using the aircraft dynamic model as time update or virtual sensor, a synthetic estimate of this triplet can be obtained. More specifically, this filter uses a dynamic model of the aircraft along with the IMU outputs (specific forces and rotation rates) and GPS outputs (position and velocity) to estimate V , α , and β .

A. Observability Analysis

Before we proceed to derive the equations of the synthetic air data estimator, we need to examine whether or not the V , α , and β triplets are observable from the IMU, GPS, and aircraft dynamic model data. That is, we need to perform an observability analysis. Observability is a measure of the ability to estimate the internal states of a system from observations of its outputs. A quantity that measures a system's observability at time step N is the observability gramian. For a linear system described by a dynamic model of the form

$$\mathbf{x}_{k+1} = \Phi_k \mathbf{x}_k + \Gamma_k \mathbf{w}_k \quad (3)$$

and a measurement model of the form

$$\mathbf{y}_k = H_k \mathbf{x}_k + \mathbf{v}_k \quad (4)$$

where \mathbf{w}_k and \mathbf{v}_k are zero-mean white noise sequences, the observability gramian \mathcal{O} (a matrix) is defined as

$$\mathcal{O}_N = H_0^T H_0 + \sum_{k=1}^N \Phi_{k-1,0}^T H_k^T H_k \Phi_{k-1,0} \quad (5)$$

where $\Phi_{k-1,0}$ is the state transition matrix from time 0 to time $k - 1$. A full-rank observability gramian matrix indicates complete observability, meaning the entire state vector can be estimated using the observations.

In some instances, observability can be assessed informally without having to compute the gramian \mathcal{O} . We present one such heuristic argument with regards to the synthetic air data estimator. In the 2-D case in which the aircraft's motion is restricted to the North-East plane as illustrated in Fig. 3, the ground speed (V_N for the North component and V_E for the East component) and airspeed (u and v along the body x and y axes, respectively) are related through the following equations:

$$V_N(t) = u(t) \cos \psi(t) - v(t) \sin \psi(t) + \tilde{W}_N(t) \quad (6a)$$

$$V_E(t) = u(t) \sin \psi(t) + v(t) \cos \psi(t) + \tilde{W}_E(t) \quad (6b)$$

where ψ is the heading angle, and \tilde{W}_N and \tilde{W}_E are the wind components along the North and East direction. Assuming constant airspeed, steady atmosphere, and ψ are known, Eq. (6) can be cast in a matrix form as follows:

$$\begin{bmatrix} V_N(t_1) \\ V_E(t_1) \\ V_N(t_2) \\ V_E(t_2) \end{bmatrix} = \underbrace{\begin{bmatrix} \cos \psi(t_1) & -\sin \psi(t_1) & 1 & 0 \\ \sin \psi(t_1) & \cos \psi(t_1) & 0 & 1 \\ \cos \psi(t_2) & -\sin \psi(t_2) & 1 & 0 \\ \sin \psi(t_2) & \cos \psi(t_2) & 0 & 1 \end{bmatrix}}_H \begin{bmatrix} u \\ v \\ \tilde{W}_N \\ \tilde{W}_E \end{bmatrix} \quad (7)$$

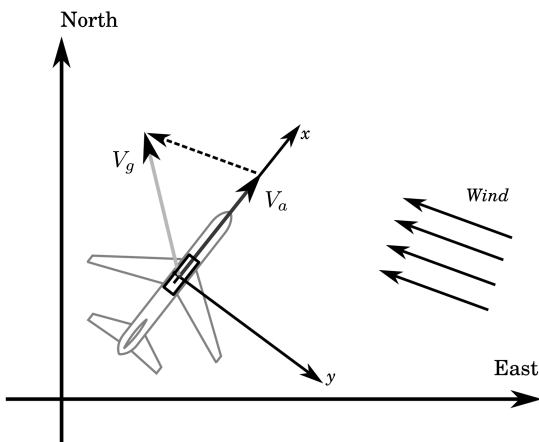


Fig. 3 Relationship between airspeed, ground speed, and wind.

Simple as it may seem, this is close to a typical case of a steady-level flight, which often constitutes a major portion of a typical flight. When $\psi(t_1) \neq \psi(t_2)$, H is full rank and can be inverted to estimate u , v , \tilde{W}_N , and \tilde{W}_E . In this case, $V = \sqrt{u^2 + v^2}$, and $\beta = \arcsin \frac{v}{V}$. Therefore, it is possible to estimate the airspeed from the ground speed observation when there is a change in the aircraft's heading. Conversely, the airspeed is not observable during a straight flight. This is an inherent limitation of the synthetic air data estimation. It is not a significant concern in most small UAVs' operations because there are usually large enough heading changes in a typical mission. Flights with prolonged straight-and-level profiles will have to make periodic small heading changes (e.g., S-turns) when using the synthetic air data system. When extended to the three-dimensional case, a change in attitude is required for observability. The constant airspeed and steady atmosphere assumptions can be relaxed when its variation with time is known or when an appropriate time-update process is incorporated to the estimator.

Hence, essential to estimate dynamically changing V , α , and β is the ability to predict their changes with time. Airspeed changes can be calculated from the aircraft's acceleration, \mathbf{a} , as measured by an accelerometer triad. The difficulty in doing this arises from the fact that the acceleration measurement is corrupted by various inertial sensor errors such as the scale factor error, κ ; turn-on bias, \mathbf{b}_a ; bias instability, \mathbf{b}_1 ; and other random noise, \mathbf{n} . This random noise, although often modeled as white noise, in reality can be colored. Mathematically, the accelerometer output \mathbf{f} can be written as follows:

$$\mathbf{f} = (I + \kappa)(\mathbf{a} - \mathbf{g}) + \dot{\tilde{\mathbf{W}}} + \mathbf{b}_a + \mathbf{b}_1 + \mathbf{n} \quad (8)$$

The bias instability \mathbf{b}_1 represents the stochastic part of the bias. The wind error $\tilde{\mathbf{W}}$ is stochastic in nature as described in [19,21]. Hence, without another piece of information, it is extremely difficult to separate sensor error from atmospheric disturbances. Even when dealing with an ideal inertial sensor that has a very stable bias (i.e. $\mathbf{b}_1 \approx 0$), the presence of the wind, as will be explained in the following section, results in a very challenging estimation problem.

The use of a flight dynamic model serves to separate the effect of inertial sensor bias from wind changes. It is an independent information of the aircraft's acceleration using the relationship between the known control input applied to the aircraft and its corresponding response. The airspeed derived from the flight dynamic model is similar to the current standard practice of using a pitch-power table when flying under instrument flight rules with an unreliable airspeed indicator. Available in this table is the airspeed that corresponds to a certain configuration (power setting, pitch attitude, weight, and altitude) [22]. In the estimator setting described in this paper, this extra information helps discriminate the inertial sensor biases from the atmospheric disturbances.

B. Filter Mechanizations

There are several sensor fusion architecture options that can be used to mechanize an estimator that generates a synthetic estimate of V , α , and β . However, as will be discussed shortly, depending on the quality of the IMU used, some architectures will yield an inaccurate estimate. In some instances, it may also result in divergence and instability of the filter. In this section, three potential different filter architectures are presented: a conventional filter, a state-constrained filter, and a cascaded, two-filter architecture. In all architectures, an EKF is used to handle the nonlinearity. The goal of this discussion is to present challenges in designing an air data estimator; in particular, we highlight the difficulties that arise when using low-cost inertial sensors with relatively large output errors and low-fidelity dynamic models of the aircraft. Stated differently, we want to show why using prior sensor fusion approaches such as [3,9–11,13] might yield poor results when used with low-cost inertial sensors.

1. Conventional Kalman Filter Architecture

A straightforward mechanization of an V , α , and β estimator would have in its state vector the following quantities:

$$\mathbf{x} = \left[\underbrace{u \ v \ w}_{\text{Airspeed}} \ \underbrace{p \ q \ r}_{\text{Rate}} \ \underbrace{\phi \ \theta \ \psi}_{\text{Attitude}} \ \underbrace{\tilde{W}_N \ \tilde{W}_E}_{\text{Wind}} \ \underbrace{L \ \Lambda \ h}_{\text{Position}} \ \underbrace{b_{ax} \ b_{ay} \ b_{az}}_{\text{AccelBias}} \ \underbrace{b_{gx} \ b_{gy} \ b_{gz}}_{\text{GyroBias}} \right] \quad (9)$$

The first six states, namely, the three components of the airspeed vector in the body axis and the angular rates, would be obtained using the aircraft dynamic model. The aircraft's position would be updated using the ground speed calculated from the vector addition of the airspeed vector and the wind components. The wind and sensor biases (accelerometers and gyros) would be propagated using some stochastic model (e.g., random walk or Gauss-Markov processes). Inertial sensor outputs and GPS outputs would be used as measurements to update the states. The measurement vector would contain the following:

$$\mathbf{y} = \left[\underbrace{f^x \ f^y \ f^z}_{\text{Accel}} \ \underbrace{\omega^x \ \omega^y \ \omega^z}_{\text{Gyros}} \ \underbrace{V_N \ V_E \ V_D \ L \ \Lambda \ h}_{\text{GPS}} \right] \quad (10)$$

They are related to the states as follows:

$$\begin{bmatrix} f^x \\ f^y \\ f^z \end{bmatrix} = \begin{bmatrix} X(u, v, w, p, q, r) \\ Y(u, v, w, p, q, r) \\ Z(u, v, w, p, q, r) \end{bmatrix} + \begin{bmatrix} b_{ax} \\ b_{ay} \\ b_{az} \end{bmatrix} \quad (11a)$$

$$\begin{bmatrix} \omega^x \\ \omega^y \\ \omega^z \end{bmatrix} = \begin{bmatrix} p \\ q \\ r \end{bmatrix} + \begin{bmatrix} b_{gx} \\ b_{gy} \\ b_{gz} \end{bmatrix} \quad (11b)$$

$$\begin{bmatrix} V_N \\ V_E \\ V_D \end{bmatrix} = C_B^N \begin{bmatrix} u \\ v \\ w \end{bmatrix} + \begin{bmatrix} \tilde{W}_N \\ \tilde{W}_E \\ 0 \end{bmatrix} \quad (11c)$$

where C_B^N indicates the transformation matrix from the body axis (i.e., the B frame) to the locally level NED coordinate frame (i.e., the N frame). This architecture is similar to that described in Wise [13] in terms of the use of IMU specific force and rate gyro outputs in the measurement equation. Wise also includes pitch and roll angles as measurements. This is not possible when MEMS-based gyroscopes are used to derive the attitude. Additionally, when the output of the same triad of gyroscopes used to generate the attitude is also used in the measurement vector, the correlation between these quantities must be accounted for.

This conventional mechanization of a synthetic air data estimator poses several problems that limit its usefulness. First, Eqs. (11a) and (11b) confound the unmodeled system errors with inertial sensor biases. In fact, having IMU outputs as measurements degrades observability because most of the errors are absorbed by the sensor biases. Second, there is a lack of correlation between the aircraft dynamics and attitude; the aircraft dynamics are, for example, independent of the aircraft's heading. This degrades the attitude observability from GPS position and velocity measurements. Third, the north and east components of the wind velocity are equivalent to the bias terms that can account not only for the velocity error but also the attitude error, which results in poor attitude and airspeed estimates. The filter can be made to work by adding attitude measurements to the measurement vector in Eq. (10).

2. State-Constrained Kalman Filter

From the preceding discussion, it is obvious that the roots of the problems that make the single estimator architecture above impractical are the attitude and the wind. Because all attitude states are not observable from aircraft dynamics alone, it seems reasonable to formulate this filter in such a way that an INS appears explicitly in the time-update process. This mechanization is slightly more complex because it requires constrained Kalman filtering techniques [23]. The state vector will have the following elements: three airspeed

components (u , v , and w), the attitude parameters (e.g., the Euler angles ϕ , θ , and ψ), three ground speed components (V_N , V_E , and V_D), three elements of position (e.g., L , Λ , and h), inertial sensor biases (three accelerometer biases and three gyro biases), and two wind components (\tilde{W}_N and \tilde{W}_D). Attitude, ground speed, and position will be propagated using conventional INS equations [7,8]. Airspeed components can be propagated using aircraft dynamics. Because gyro outputs are available in the time-update process (used for attitude propagation), rotational dynamics of the aircraft are not necessary. Any dependencies on the body rate (p , q , and r) will use the corresponding rate gyro outputs corrected for their respective biases. Inertial sensor biases and wind would be propagated using a stochastic model. The GPS position and velocity are used as measurements. In addition, because ground speed, airspeed, and wind are related through Eq. (11c), the perfect measurement techniques [23] can be applied to enforce this relationship:

$$\mathbf{y} = \mathbf{h}(\mathbf{x}) + \mathbf{n}_y = \mathbf{C}_B^N \begin{bmatrix} u \\ v \\ w \end{bmatrix} + \begin{bmatrix} \tilde{W}_N \\ \tilde{W}_E \\ 0 \end{bmatrix} - \begin{bmatrix} V_N \\ V_E \\ V_D \end{bmatrix} + \mathbf{n}_y = \begin{bmatrix} 0 \\ 0 \\ 0 \end{bmatrix} \quad (12a)$$

$$\mathbb{E}(\mathbf{n}_y) = \mathbf{0}, \quad \mathbb{E}(\mathbf{n}_y \mathbf{n}_y^T) = \mathbf{0} \quad (12b)$$

There are several drawbacks to this method. The sensor bias model in the INS/GPS filter acts like an integrator that keeps the innovation small. However, it is widely known that, due to the unavailability of a high-fidelity sensor-error model for low-cost MEMS inertial sensors, the sensor bias estimate does not, in general, represent the true measurement bias in the output [8]. Other unmodeled error sources such as the scale factor and misalignment errors will be absorbed by the sensor bias states. When the rate gyro output is corrected using its bias estimate and used in the aircraft dynamics propagation equation, the resulting attitude estimate will be inaccurate. Another drawback of using this method is that imperfect aircraft models will affect the accuracy of other states. States such as position and attitude, which can be estimated well by fusing INS with GPS measurements alone, may suffer the detrimental effect of having inaccurate aircraft dynamic model.

3. Cascaded Filter Architecture

A very similar problem to the one discussed in this paper (from a filter design point of view) was encountered in a ground vehicle application [24] in which a conventional Kalman filter architecture was unable to estimate attitude and gyro bias during GPS outages. In that work, a cascaded filter architecture was used to constrain the estimation of different bias terms to their respective subsystem. It was shown that this method improves the quality of the estimates in GPS outages during which the heading was unavailable (it was estimated using a multiple-antenna GPS system). Breaking a problem that involves estimating several bias terms into two filters is not new. This approach has been studied in other context in the past [25,26] and formally justified in [27].

In view of the preceding noted prior work, we propose a cascaded, two-filter architecture along the line of [24] to constrain sensor biases and wind states. In this formulation of the synthetic airspeed estimator, the low-cost INS is fused with the GPS in one filter. This filter generates an estimate of the airplane's position, ground speed, and attitude as well as inertial sensor biases. Such filters are not new and have been the subject of many papers and books in the last decade [7,8,28,29]. The second filter uses the aircraft dynamic model for its time-update equations and the outputs of the first filter as its measurement vector.

Because successive outputs of the first filter are correlated, this time correlation must be accounted for explicitly in the second filter. Although these additional states complicate the structure of the estimator, the added complexity is outweighed by the ease by which one can impose state constraints, thereby ensuring reasonably accurate V , α , and β estimates. By the virtue of having separate filters

to handle each navigation and air data estimation problem, this architecture yields not only an accurate estimate of the V , α , and β triplet but also an accurate navigation solution for position, ground speed, and attitude. The separation prevents the error from the aircraft dynamic model from corrupting the navigation state estimates.

Figure 4 is a functional block diagram of the filter architecture used to estimate the airspeed, angle of attack, and sideslip. The estimation process is divided into two steps. First, the aircraft's inertial position, velocity, and attitude are estimated by fusing the information from an IMU and GPS. The ground speed and attitude estimates from this filter are then used as inputs to the second filter that decomposes the ground speed into the airspeed component and the wind component.

When the INS and GPS are combined, the blended navigation solution has the high bandwidth of the inertial sensors and the drift-free long-term stability of the GPS solution [7,8,28,29]. The INS/GPS navigation solution consists of the absolute position, velocity, and attitude that fully describe the aircraft's kinematics state. For the work described here, the INS/GPS filter is a 15-state extended Kalman filter [8]. The output of this filter is the following state vector:

$$\mathbf{x}|_{\text{Filter1}} = \begin{bmatrix} \underbrace{L \Lambda h}_{\text{Position}} & \underbrace{V_N \ V_E \ V_D}_{\text{Groundspeed}} & \underbrace{\phi \ \theta \ \psi}_{\text{Attitude}} & \underbrace{b_{ax} \ b_{ay} \ b_{az}}_{\text{AccelBias}} & \underbrace{b_{gx} \ b_{gy} \ b_{gz}}_{\text{GyroBias}} \end{bmatrix} \quad (13)$$

A subset of $\mathbf{x}|_{\text{Filter1}}$ is used as a measurement in the second filter. This is denoted $\mathbf{y}|_{\text{Filter2}}$ and is given by

$$\mathbf{y}|_{\text{Filter2}} = [V_N \ V_E \ V_D \ \phi \ \theta \ \psi] \quad (14)$$

The second filter extracts V , α , and β from the first filter using flight control inputs (throttle, elevator, aileron, and rudder) along with ground speed and attitude estimates from the first navigation filter. As has been mentioned earlier, $\mathbf{y}|_{\text{Filter2}}$ is time correlated. This time correlation will be accounted for by augmenting filter 2 with six additional states. Therefore, the state vector in the second filter consists of the following states:

$$\mathbf{x}|_{\text{Filter2}} = [u \ v \ w \ p \ q \ r \ \phi \ \theta \ \psi \ W_N \ W_E \ b_D \ b_\phi \ b_\theta \ b_\psi] \quad (15)$$

W_N , W_E , b_D , b_ϕ , b_θ , and b_ψ are terms that account for the time correlation in the measurements used in the second filter. As will be described in the following sections, W_N and W_E are called

pseudowind estimates because they include both the estimate of the wind (\tilde{W}_N and \tilde{W}_E) and the time correlation in the measurements. Aircraft dynamics are used to separate the airspeed from the wind speed and serve as the time update to the filter. The inputs that drive this process are flight control inputs (propeller rotation speed, elevator, aileron, and rudder deflections).

III. Filter Description

A. Coordinate Frames

The airspeed and ground speed are velocities of the airplane measured relative to two different coordinate frames. Equation (16) shows the relation between the two and is the key governing equation for the air data extraction from the ground speed measurement:

$$\mathbf{V}_{EB}^N = C_B^N \mathbf{V}_{WB}^B + \tilde{\mathbf{W}}^N \quad (16)$$

The superscript on the variables indicates the coordinate frame in which the vector is resolved. Superscript $(\cdot)^N$ indicates the local navigation frame, F_N , which has its x axis pointing toward true North (as opposed to magnetic North), the y axis pointing toward East, and the z axis pointing downward, completing the right-handed coordinate system. Superscript $(\cdot)^B$ indicates the body frame that is a set of axes with the origin at the aircraft's center of mass. In this coordinate frame, the x axis points forward along the fuselage, the y axis points to the right, and the z axis points downward, completing the right-handed coordinate system. The subscript indicates the frame relative to which the vector is measured. For example, the subscript $(\cdot)_{EB}$ indicates that the vector is a quantity (e.g., velocity) of F_B relative to the earth frame, F_E , and subscript $(\cdot)_{WB}$ indicates the vector is measured relative to the wind frame, F_W . The earth frame, F_E , is a frame with its origin at the center of the Earth and rotates together with the Earth, whereas the wind frame, F_W , moves together with the surrounding air mass. For low-speed subsonic flights, F_E can be assumed to be inertial, and the flat, nonrotating Earth assumption can be used.

Equation (16) is key to this synthetic airspeed system. Given the control inputs, the airspeed time evolution is calculated using aircraft dynamics. Equation (16) is used as an observation equation to

separate the wind components from the air data measurements. In the second filter, the attitude (ϕ , θ , and ψ) and body rates (p , q , and r) are estimated despite being available as inputs from the first filter. This is

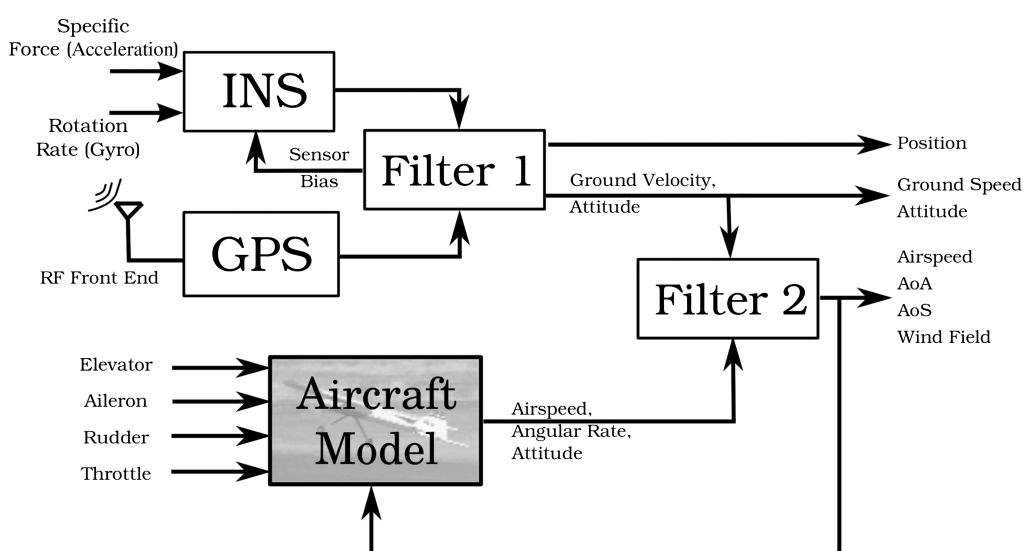


Fig. 4 Air data estimator architecture.

done to avoid a correlation between process noise and measurement noise, which would add unnecessary complexity to the filter to handle it correctly.

B. Aircraft Dynamics

Under the flat Earth assumption, the six-DOF rigid-body aircraft equations of motion can be summarized as follows [30]:

$$X - mg \sin \theta = m(\dot{u} + qw - rv) \quad (17a)$$

$$Y + mg \cos \theta \sin \phi = m(\dot{v} + ru - pw) \quad (17b)$$

$$Z + mg \cos \theta \cos \phi = m(\dot{w} + pv - qu) \quad (17c)$$

$$\mathcal{L} = I_x \dot{p} - I_{xz}(\dot{r} + pq) - (I_y - I_z)qr \quad (18a)$$

$$\mathcal{M} = I_y \dot{q} - I_{xz}(r^2 - p^2) - (I_z - I_x)rp \quad (18b)$$

$$\mathcal{N} = I_z \dot{r} - I_{xz}(\dot{p} - qr) - (I_x - I_y)pq \quad (18c)$$

$$\dot{\phi} = p + q \sin \phi \tan \theta + r \cos \phi \tan \theta \quad (19a)$$

$$\dot{\theta} = q \cos \phi - r \sin \phi \quad (19b)$$

$$\dot{\psi} = (q \sin \phi + r \cos \phi) \sec \theta \quad (19c)$$

The total airspeed vector components u , v , and w are related to the airspeed, V ; angle of attack, α ; and sideslip, β , through the following relations:

$$V = \sqrt{u^2 + v^2 + w^2} \quad (20a)$$

$$\alpha = \tan^{-1} \frac{w}{u} \quad (20b)$$

$$\beta = \sin^{-1} \frac{v}{\sqrt{u^2 + v^2 + w^2}} \quad (20c)$$

The aerodynamic forces and moments are, in general, functions of the air density, airspeed, angle of attack, sideslip, body rates, and control surface deflections, and their dependence on some of these variables is nonlinear. Assuming a small angle of attack and sideslip and that the thrust is aligned with the x_B axis, the relations for the thrust and aerodynamic forces are given as

$$T = \rho f^2 d^4 C_T \quad (21a)$$

$$X = T - \frac{1}{2} \rho V^2 S C_D \quad (21b)$$

$$Y = \frac{1}{2} \rho V^2 S C_Y \quad (21c)$$

$$Z = -\frac{1}{2} \rho V^2 S C_L \quad (21d)$$

Similarly, the propulsive and aerodynamic moments are given by

$$\mathcal{T} = -\frac{\rho f^2 d^5 C_P}{2\pi} \quad (22a)$$

$$\mathcal{L} = \mathcal{T} + \frac{1}{2} \rho V^2 S b C_l \quad (22b)$$

$$\mathcal{M} = r_z \mathcal{T} + \frac{1}{2} \rho V^2 S c C_m \quad (22c)$$

$$\mathcal{N} = -r_y \mathcal{T} + \frac{1}{2} \rho V^2 S b C_n \quad (22d)$$

Equation (22) includes the effect of eccentric thrust loading with respect to the aircraft's center of mass. The generic mathematical relationship for each coefficient for a single-piston-engine aircraft used in the simulation studies that will be presented later can be found in Appendix A.

C. Time Update

To mechanize the aircraft dynamics as a time-update process in the Kalman filtering framework, the following steps and assumptions are taken. First, taking into account the stochastic nature of the measured control inputs, the dynamics equation can be described by the following nonlinear relationship:

$$\mathbf{x}_{k+1} = \mathcal{F}(\mathbf{x}_k, f + n_{f,k}, \delta_{e,k} + n_{e,k}, \delta_{a,k} + n_{a,k}, \delta_{r,k} + n_{r,k}) \quad (23)$$

where \mathcal{F} represents the nonlinear relationship given by Eqs. (17–19). n_f , n_e , n_a , and n_r are noise on the measurements of propeller rotation speed, elevator deflection, aileron deflection, and rudder deflection, respectively. They are assumed to be discrete white noise sequences [31] with standard deviations σ_f , σ_e , σ_a , and σ_r , respectively. The statistics of the noise sequence are used to construct the process noise power-spectral density matrix, R_w , as discussed next.

As mentioned in the preceding discussion, the measurements fed to the second filter have errors that are time correlated. The second filter must then account for this correlation because failure to do so may result in a suboptimal filter that possibly outputs inaccurate estimates or an overly confident covariance. There are several methods that have been studied in the past to account for this correlated error explicitly [32]. The most common way is by augmenting the state vector with terms that model the correlation. One of these models is the first-order Gauss–Markov model:

$$\dot{\mathbf{b}} = -\frac{1}{\tau} \mathbf{b} + \mathbf{n} \quad (24)$$

In reality, the correlation may consist of several first or higher order processes. This first-order model is a simple yet effective way to overbound an actual stochastic process. By tuning the time constant τ and the power-spectral density of the Gaussian white noise n , it is possible to generate a conservative estimate of the process [33]. This is the reason why this model is used very frequently to model an unknown but slowly varying stochastic signal. For example, it has been used successfully in [19–21] to model the wind speed variation. This paper adopts the first-order Gauss–Markov process to model the correlated errors in the measurements as well as changes in wind speed.

Because there are six measurements (three ground speed components and three Euler angles) coming into the second filter, there are six states as described in Eq. (15) that account for the time correlation of each state. Each of these states will have two parameters associated with it, namely, τ and n . Here, these errors are assumed to be uncorrelated with each other. Therefore, we have

$$\mathbb{E}[n_{(j)}(t)] = 0 \quad (25a)$$

$$\mathbb{E}[n_{(\cdot)}(t)n_{(\cdot)}(t + \Delta t)] = \sigma_{(\cdot)}^2 \underline{\delta}(\Delta t) \quad (25b)$$

$$\mathbb{E}[n_{(\cdot)}(t)n_{(\times)}(t)] = 0 \quad (25c)$$

Equations (17–24) can be recast into the following discrete, state-space form, as described in any standard estimation text [32]:

$$\hat{\mathbf{x}}_{k+1} = \mathcal{F}(\hat{\mathbf{x}}_k, f, \delta_{e,k}, \delta_{a,k}, \delta_{r,k}) \quad (26a)$$

$$P_k = \Phi_{k-1} P_{k-1} \Phi_{k-1}^T + Q_{k-1} \quad (26b)$$

where Φ_k is the discrete-time equivalent of the Jacobian matrix, and Q_k is the discrete-time equivalent of the process noise covariance matrix. They are calculated using

$$\Phi_k = e^{(F_k T_s)} \quad (27a)$$

$$Q_k = G_k R_w G_k^T T_s \quad (27b)$$

where T_s is the sampling time [34]. F_k denotes the Jacobian matrix of \mathcal{F} , R_w denotes the power-spectral density of the noises on the control surface deflection, and G denotes the noise-shaping matrix obtained through the linearization of \mathcal{F} with respect to the control surface deflections.

The Jacobian F and the shaping matrix G are given in Appendix B. The power-spectral density R_w is given as

$$\mathbf{R}_w = \begin{bmatrix} \sigma_e^2 & 0 & 0 & 0 & 0 & 0 & 0 & 0 & 0 & 0 \\ 0 & \sigma_a^2 & 0 & 0 & 0 & 0 & 0 & 0 & 0 & 0 \\ 0 & 0 & \sigma_r^2 & 0 & 0 & 0 & 0 & 0 & 0 & 0 \\ 0 & 0 & 0 & \sigma_f^2 & 0 & 0 & 0 & 0 & 0 & 0 \\ 0 & 0 & 0 & 0 & \frac{2\sigma_w^2}{\tau_w} & 0 & 0 & 0 & 0 & 0 \\ 0 & 0 & 0 & 0 & 0 & \frac{2\sigma_w^2}{\tau_w} & 0 & 0 & 0 & 0 \\ 0 & 0 & 0 & 0 & 0 & 0 & \frac{2\sigma_{wD}^2}{\tau_{wD}} & 0 & 0 & 0 \\ 0 & 0 & 0 & 0 & 0 & 0 & 0 & \frac{2\sigma_{w\phi}^2}{\tau_{w\phi}} & 0 & 0 \\ 0 & 0 & 0 & 0 & 0 & 0 & 0 & 0 & \frac{2\sigma_{w\theta}^2}{\tau_{w\theta}} & 0 \\ 0 & 0 & 0 & 0 & 0 & 0 & 0 & 0 & 0 & \frac{2\sigma_{w\psi}^2}{\tau_{w\psi}} \end{bmatrix} \quad (28)$$

D. Measurement Update

As noted earlier, the key to synthetic air data estimation lies in Eq. (16). This equation relates the ground speed, \mathbf{V}_{EB}^N , and attitude, C_N^B , estimates from the first filter with the information provided by the aircraft dynamic model. After augmenting the state with six additional correlated error states, the nonlinear measurement equation can be written as

$$\begin{bmatrix} V_N \\ V_E \\ V_D \\ \phi \\ \theta \\ \psi \end{bmatrix}_{\text{Filter1}} = \begin{bmatrix} C_B^N & 0_{3 \times 3} \\ 0_{3 \times 3} & I_{3 \times 3} \end{bmatrix} \begin{bmatrix} u \\ v \\ w \\ \dot{\phi} \\ \dot{\theta} \\ \dot{\psi} \end{bmatrix} + \begin{bmatrix} W_N \\ W_E \\ b_D \\ b_\phi \\ b_\theta \\ b_\psi \end{bmatrix} + \mathbf{n}_y \quad (29)$$

where \mathbf{n}_y denotes the measurement noise or the uncertainty in the ground speed and attitude measurements. After separating the time correlated error from the total uncertainty in the measurement, \mathbf{n}_y can be assumed to be uncorrelated in time (i.e. white) but still correlated

with each other. This interstate correlation is captured in the state covariance from the first filter, and hence, the measurement noise covariance matrix $R = \mathbb{E}(\mathbf{n}_y \mathbf{n}_y^T)$ can be extracted from it. Mathematically,

$$R = \mathbb{E}(\mathbf{n}_y \mathbf{n}_y^T) = P_{\text{Filter1}}[4:9, 4:9] \quad (30)$$

Equation (29) is nonlinear. Hence, the ground speed vector, \mathbf{y}_{GS} , and attitude vector, \mathbf{y}_Ψ , are linearized as follows:

$$\delta \mathbf{y}_{GS} = \mathbf{V}_{EB}^N|_{\text{Filter1}} - (\hat{C}_B^N \hat{\mathbf{V}}_{WB}^B + \hat{\mathbf{W}}^N) \quad (31)$$

$$\delta \mathbf{C}^\vee = C_B^N|_{\text{Filter1}} \hat{C}_N^B - I_{3 \times 3} \quad (32a)$$

$$\begin{aligned} \delta \mathbf{y}_\Psi &= [\delta \phi \quad \delta \theta \quad \delta \psi]^T \\ &= [-\delta C(2, 3) \quad \delta C(1, 3) \quad -\delta C(1, 2)]^T \end{aligned} \quad (32b)$$

Defining the linearized measurement vector as

$$\delta \mathbf{y} = [\delta \mathbf{y}_{GS} \quad \delta \mathbf{y}_\Psi]^T \quad (33)$$

the linearized measurement equation can be written as

$$\delta \mathbf{y} = H \delta \mathbf{x} + \mathbf{n}_y \quad (34a)$$

$$H = \begin{bmatrix} \hat{C}_B^N & 0_{3 \times 3} & [(\hat{C}_B^N \hat{\mathbf{V}}_{WB}^B) \times] & I_{3 \times 3} & 0_{3 \times 3} \\ 0_{3 \times 3} & 0_{3 \times 3} & I_{3 \times 3} & 0_{3 \times 3} & I_{3 \times 3} \end{bmatrix} \quad (34b)$$

The measurement update at time step k is done as follows:

$$K_k = P_k^- H_k^T (H_k P_k^- H_k^T + R_k)^{-1} \quad (35a)$$

$$\hat{\mathbf{x}}_k^+ = \hat{\mathbf{x}}_k^- + K_k \delta \mathbf{y}_k \quad (35b)$$

$$P_k^+ = (I - K_k H_k) P_k^- \quad (35c)$$

A block diagram that describes the filter implementation can be found in Appendix D.

IV. Validation and Simulation Study

The synthetic air data system algorithm described before was validated using a series of simulation flight tests. To examine the filter performance, the filter is run using simulated flight data obtained by using an ATC 710 M flight simulator. It is a single-engine Federal Aviation Administration level 3 flight training device that uses Flight Gear as its core simulator. We simulated a Cessna 172 maneuvering at an altitude of 1000 ft. The aerodynamic model of the aircraft

Table 1 Simulated maneuvers

Maneuver	Time, s	Description
1	200–400 500–600 1000–1200	Level flight with 30 deg bank turns at 100 kt
2	400–500	Steep 50 deg bank turns at 100 kt
3	600–800	Level flight with 30 deg bank turns at 70 kt
4	800–950	Level flight with 30 deg bank turns at 80 kt

is known from the aircraft configuration files. Appendix A shows the aerodynamic coefficients used in the force and moment computations. The simulated maneuvers are shown in Table 1.

Some of these are aggressive maneuvers in that they involve large changes in the angle of attack, sideslip, and attitude. Because the simulator was handflown, the numbers mentioned in Table 1 are approximate values as the true value changes during the maneuver as a function of pilot skill. Figure 5 depicts the simulation trajectories. In the simulation, the wind was blowing from the North at 10 kt.

Although the first filter runs as soon as the GPS solution exists, the second filter due to its use of aircraft dynamics can only run after the aircraft is airborne. There are two ways in which we can detect whether the airplane is airborne. First, we can assume that airplane is not airborne until the speed is about 1.2 times greater than the airplane's stall speed. An alternative method would be to start the second filter by looking at the first time the aircraft has a positive climb rate. The first approach is used in this simulation. The first filter runs independently of the second filter, and as soon as the aircraft gets airborne, the second filter is initialized in the following manner:

$$\hat{u} = (\sqrt{V_N^2 + V_E^2 + V_D^2})_{\text{Filter1}}, \quad \hat{v} = \hat{w} = 0 \quad (36a)$$

$$\begin{aligned} \hat{p} &= \omega^x - b_{ax}|_{\text{Filter1}}, & \hat{q} &= \omega^y - b_{ay}|_{\text{Filter1}}, \\ \hat{r} &= \omega^z - b_{az}|_{\text{Filter1}} \end{aligned} \quad (36b)$$

$$\hat{\phi} = \phi|_{\text{Filter1}}, \quad \hat{\theta} = \theta|_{\text{Filter1}}, \quad \hat{\psi} = \psi|_{\text{Filter1}} \quad (36c)$$

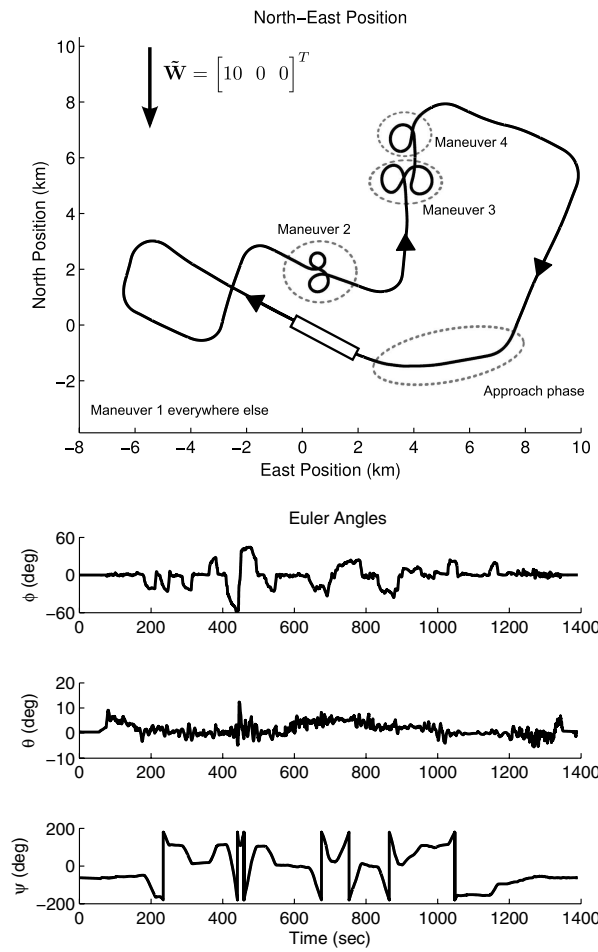


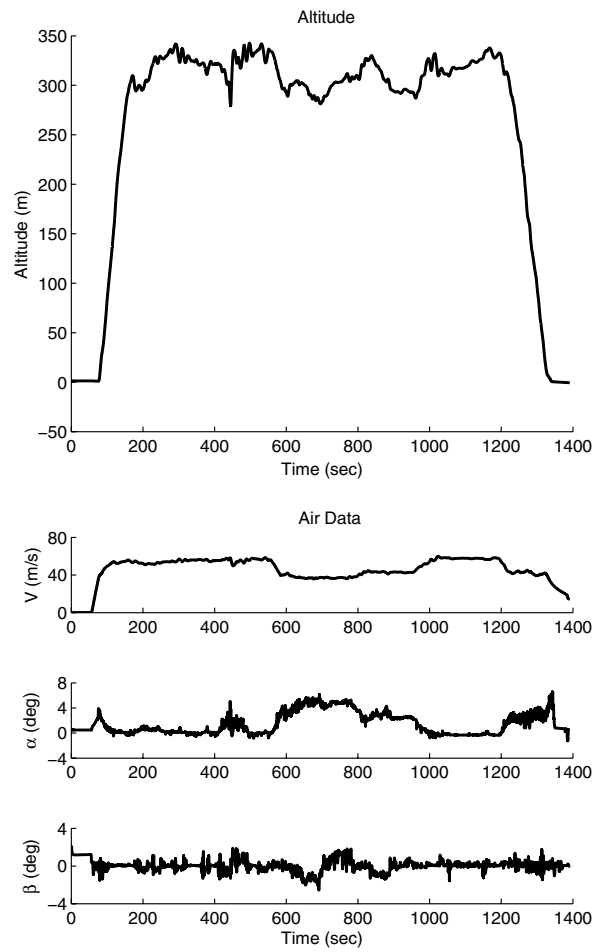
Fig. 5 Simulated trajectory: position, attitude, and air data.

$$\hat{W}_N = \hat{W}_E = \hat{b}_D = \hat{b}_\phi = \hat{b}_\theta = \hat{b}_\psi = 0 \quad (36d)$$

The initial covariance is assumed to be diagonal with components as follows:

$$\begin{aligned} P^- = \text{diag} \left[\begin{array}{c} \underbrace{(5 \text{ m/s})^2}_{\text{Airspeed}} \underbrace{(2 \text{ m/s})^2}_{\text{Body rates}} \underbrace{(2 \text{ m/s})^2}_{\dots} \\ \underbrace{(0.0087 \text{ rad/s})^2}_{\text{Attitude}} \underbrace{(0.0087 \text{ rad/s})^2}_{\text{Pseudo-wind}} \underbrace{(0.0087 \text{ rad/s})^2}_{\dots} \\ \underbrace{(3 \text{ m/s})^2}_{\text{Correlated error}} \underbrace{(3 \text{ m/s})^2}_{\dots} \end{array} \right] \end{aligned} \quad (37)$$

where the notation $P_{\text{Filter1}}[j]$ is used to indicate the variance of the j th state in the first filter. In reality, the diagonal assumption on the initial covariance matrix is not generally true. However, the correlations among the initial states are often unavailable. The common practice is to let the filter resolve the correlation as it approaches steady state. The initial covariance of the airspeed should reflect the uncertainty of the wind field around the aircraft. Although the filter is not very sensitive to the initial variances of the airspeed and wind states, overconfidence on the initial wind estimate (i.e. small variance) leads to a slower convergence. The variances of the body rates are initialized using the noise level on the rate gyro used in the simulation. On the other hand,



because the attitude is initialized as is using the first filter estimates, its variance can be directly taken from the first filter.

In this simulation, the flight control sampling frequency is 50 Hz ($T_s = 0.02$ s), and the measurement update of the synthetic air data system runs at 2.5 Hz. The process noise covariance and correlation times of the correlated error states are used as the filter tuning parameters. This technique is commonly used to account for modeling uncertainty and linearization error. The result shown here will be for the following process noise parameters:

$$\sigma_e = \sigma_a = \sigma_r = 0.4 \text{ deg} \quad (38a)$$

$$\sigma_f = 400 \text{ rpm} \quad (38b)$$

$$\sigma_{w_N} = \sigma_{w_E} = 0.05 \text{ m/s}, \quad \tau_{w_N} = \tau_{w_E} = 1 \text{ s} \quad (38c)$$

$$\sigma_{b_D} = 0.02 \text{ m/s}, \quad \tau_{b_D} = 100 \text{ s} \quad (38d)$$

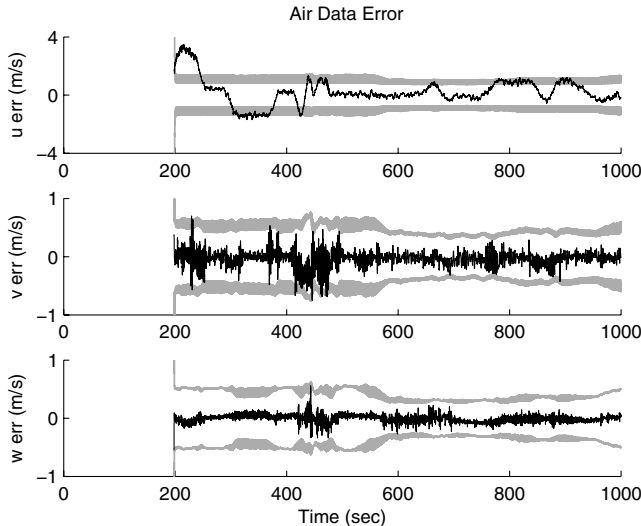


Fig. 6 Sim C172: air data estimates. Gray lines are 3σ bound.

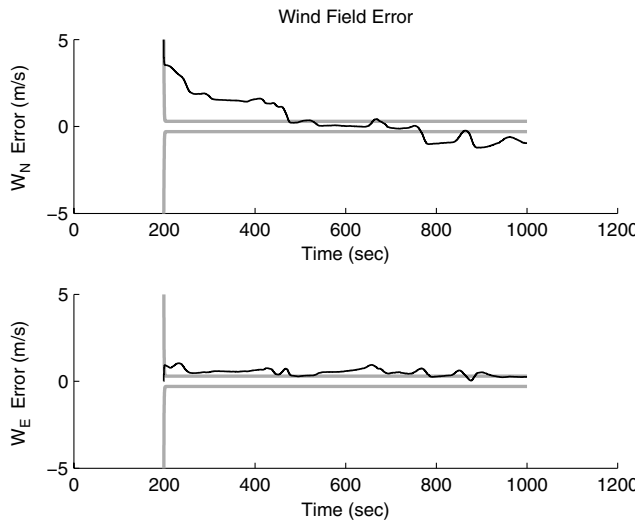


Fig. 7 Sim C172: pseudowind estimates. Gray lines are 3σ bound.

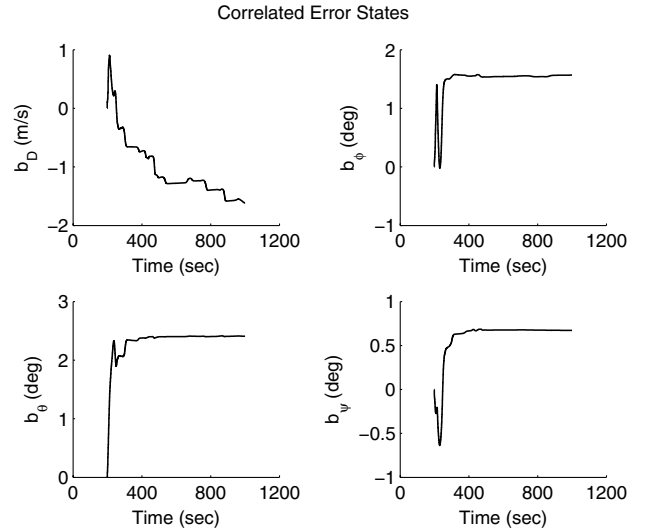


Fig. 8 Sim C172: correlated error estimates.

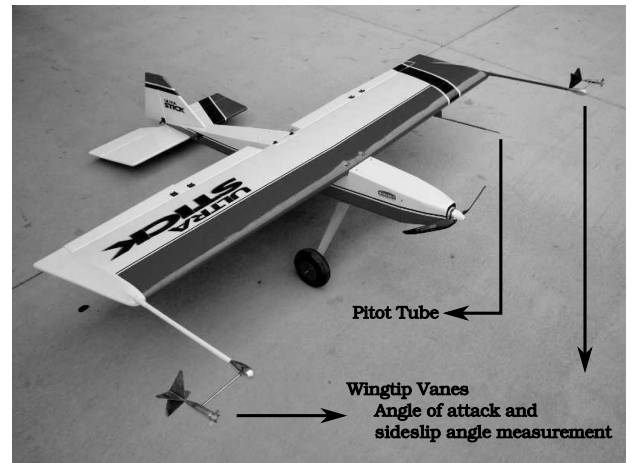


Fig. 9 Ultrastick 120.

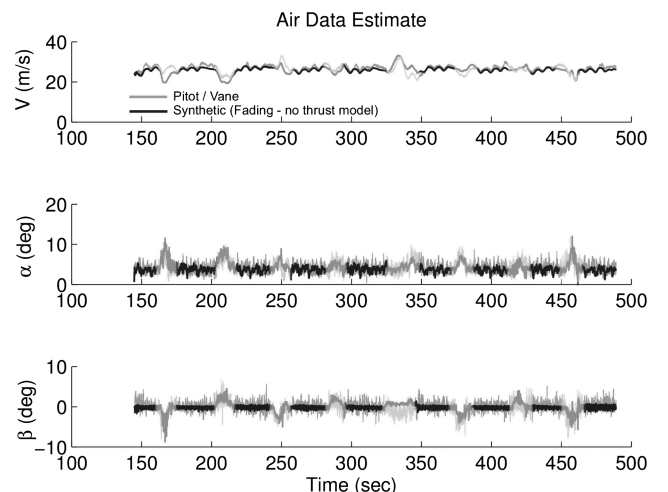


Fig. 10 Flight-test FASER: airspeed, angle of attack, and sideslip angle estimates.

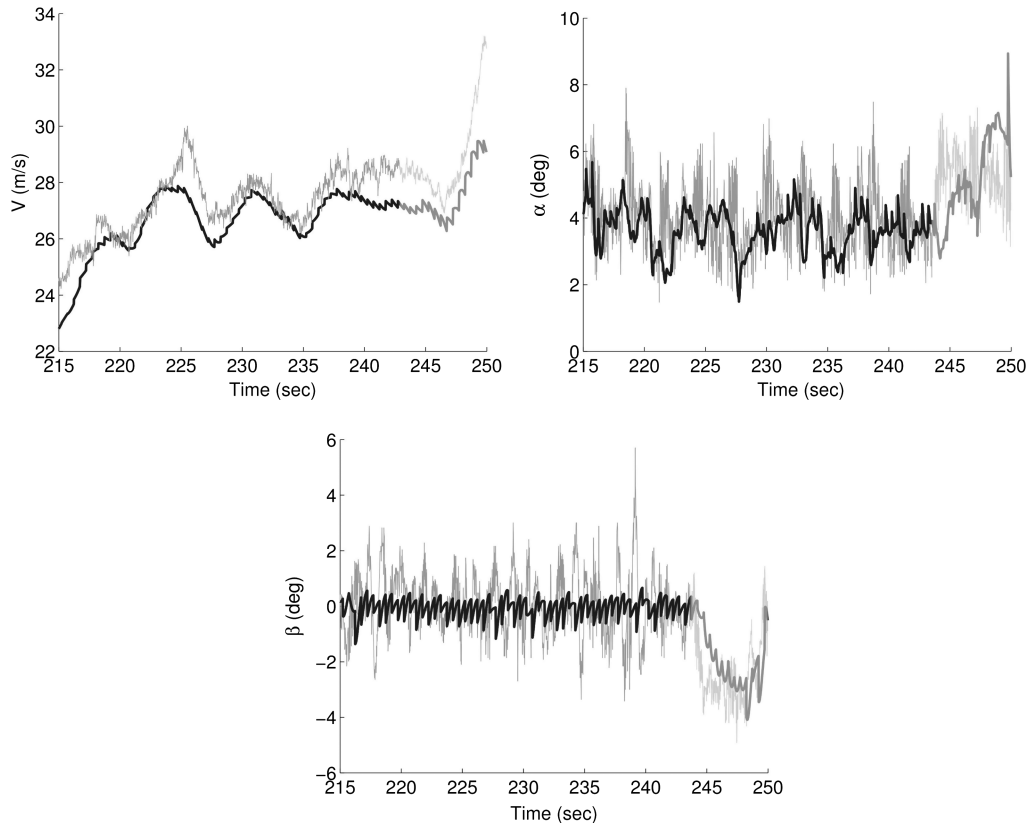


Fig. 11 Close-up on the V , α , and β estimates of FASER's flight test.

$$\sigma_{b_\phi} = \sigma_{b_\theta} = \sigma_{b_\psi} = 0.01 \text{ deg}, \quad \tau_{b_\phi} = \tau_{b_\theta} = \tau_{b_\psi} = 100 \text{ s} \quad (38e)$$

Figures 6 and 7 depict the estimation error of the total airspeed vector components (u , v , and w) and estimation error of the pseudowind, respectively. Figure 6 plots u , v , and w instead of V , α , and β to show the 3σ -bound plot obtained from the filter. Equation (20) can be used to transform the quantities to the desired form. The root mean square error of the u , v , and w estimates are 0.93, 0.14, and 0.06 m/s, respectively. Maximum errors of 3.49, 0.75, and 0.56 m/s for the three respective estimates were observed during the initial transient after filter 2 starts generating estimate. It can be attributed to the straight line trajectory during which the airspeed and wind are not separable. Soon after the first turn is initiated, the error is in agreement with the 3σ bound.

The synthetic air data system seems to generally produce estimates that are accurate except during high angle of attack maneuvers. Perhaps this is because during these maneuvers, the error that comes from small-angle approximations in the aircraft dynamic model contributes to the error in the state estimates. The wind estimates, as shown in Fig. 7, converge somewhat closely to the nominal value set up in the simulation. The error/bias and variation in the estimates are due to the fact that they also account for other unmodeled error in filter 2. Figure 8 depicts the estimates of the time correlated error in the measurements that come into filter 2.

V. Flight Test

Experimental validation of the synthetic air data estimator was accomplished by postprocessing the flight-test data collected on an Ultrastick 120 testbed. The goal of this process was to compare the performance of the synthetic air data system against the traditional air data system installed on the aircraft. The Ultrastick 120 used is a small uninhabited aerial vehicle formerly operated by NASA under the name FASER or Free-flying Aircraft for Subscale Experimental Research [35]. The airframe is a low-cost fixed-wing radio-controlled aircraft with standard elevator, aileron, and rudder control surfaces.

The UAV is powered by an electric motor that drives a propeller. Appendix C summarizes the aerodynamic and physical properties of the Ultrastick 120, and the dynamic model for the UAV is also shown there. It is equipped with an Analog Device ADIS16405 IMU and a Hemisphere Crescent GPS receiver as primary navigation sensors. The air data system consists of AMS 5812 pressure transducers that make up the pitot-static system and wingtip vanes [36] to measure angle of attack and sideslip angle (Fig. 9). Analog potentiometers are used to measure the actual control surface deflection in flight. More information on the UAV testbed can be found on the University of Minnesota's UAV Laboratory website[§].

In this FASER testbed used for these flight tests, measurements of all the control inputs except for throttle setting were available. Thus, the throttle setting was estimated as follows. The throttle setting used when flying straight and level is known, and the value for this fixed throttle setting is predetermined on the ground to achieve straight-and-level flight conditions. The major portion of the flight was executed at this throttle setting, and the constant thrust assumption can be made. However, throttle change is inevitable whenever the UAV executes turns. During these transient maneuvers, the constant thrust assumption is violated. At these moments, the dynamic model's fidelity is reduced. As will be shown later, this causes transient errors in the air data estimates.

Because this constant thrust assumption for the major portion of the flight and small commanded pitch changes, linearized aircraft dynamics can be used for the second filter time update [Eq. (23)]. Postflight inspection of the flight data showed that the aircraft maneuvered close to the trim velocity of 26.5 m/s.

The filter is initialized similarly to the simulation [Eqs. (36–38)]. Equation (39) gives the values used for these process noise variables. The differences in the parameters used for flight tests and simulation are expected due to the different aircraft platform used in these two studies:

[§]Data available online at <http://www.uav.aem.umn.edu> [retrieved 13 March 2013].

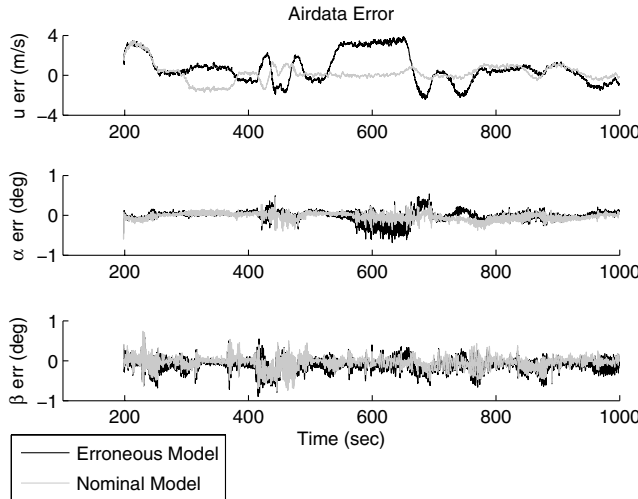


Fig. 12 Air data estimates with wrong C_T and C_P .

$$\sigma_e = \sigma_a = \sigma_r = 0.5 \text{ deg} \quad (39a)$$

$$\sigma_{w_N} = \sigma_{w_E} = 0.05 \text{ m/s}, \quad \tau_{w_N} = \tau_{w_E} = 1 \text{ s} \quad (39b)$$

$$\sigma_{b_D} = 0.02 \text{ m/s}, \quad \tau_{b_D} = 100 \text{ s} \quad (39c)$$

$$\sigma_{b_\phi} = \sigma_{b_\theta} = \sigma_{b_\psi} = 0.01 \text{ deg}, \quad \tau_{b_\phi} = \tau_{b_\theta} = \tau_{b_\psi} = 100 \text{ s} \quad (39d)$$

The flight control sampling frequency and measurement update rate on the synthetic air data system run at 50 and 2.5 Hz, respectively.

Figure 10 depicts the state estimates from the filter compared against the measured values from the pitot-static/vane air data system. It can be seen that the accuracy of the airspeed estimate is reasonably good in the portion of the flight in which the throttle settings were fixed but poor during maneuvers that require the thrust to be varied (faded time slices in Fig. 10). This poor accuracy can be attributed to the lack of a throttle-to-airspeed relationship in the linearized state-space model. On the other hand, the angle of attack and sideslip compare pretty well with the vane readings. A close up depiction of these estimates is shown in Fig. 11.

This result shows that it is possible to generate a reasonably accurate synthetic air data estimate using a simplified dynamic model. In particular, the synthetic air data estimate can be generated using a linear model of the aircraft. This linear model is generated

by linearizing the aircraft about a straight-and-level flight at a particular airspeed (trim). Therefore, there are infinitely many linear models that can be obtained throughout the entire flight envelope. In this work, we have not quantified the accuracy of the synthetic air data estimate when an incorrect linear model is used. Analysis on the range of validity of a linear model is the subject of ongoing work.

VI. Sensitivity to Aerodynamic Parameters

At the beginning of this paper, it was noted that the motivation for developing the synthetic air data system was the need to enhance the integrity of existing air data systems through analytical redundancy. For commercial and general aviation aircraft as well as large military UAVs (e.g., Predator or Globalhawk), the aircraft dynamic model used to estimate V , α , and β is likely to be accurate and change very little in operation. This is because, in part, such aircraft have little variation in the manufacturing process and usually have gone through a lengthy and expensive testing process. This process ensures that an accurate aircraft model validated by performance data is available.

For low-cost platforms such as small, hand-launched UAVs, this may not be the case. Thus, inaccuracies or unmodeled changes of the dynamic model may lead to a poor estimation of V , α , and β . The effect can be rather complicated, especially when we consider the fact that the nonlinear time-update equations [Eqs. (17–19)] are linearized about estimates generated by the synthetic system. This is the subject of ongoing work and beyond the scope of this work. For completeness, however, we present some preliminary results regarding the sensitivity of V , α , and β estimates to inaccurate or unmodeled changes of the dynamic model.

Figure 12 shows the estimation error of the same flight scenario as described in Sec. IV but using an erroneous thrust model. The error in thrust model is introduced by perturbing C_T and C_P by 10%. This error is an upper bound on the variations in C_T and C_P observed in wind-tunnel experimental results documented in Fig. 13. Figure 12 shows that airspeed estimate is more sensitive to the thrust model errors than the angle of attack and sideslip estimates.

A thorough sensitivity analysis would examine the effect of individual parameter errors on the estimation error. Although it is straightforward to appreciate that C_T and C_P errors will cause V , α , and β estimate errors, it may not be apparent that the effect is stochastic and not deterministic in nature. To see this, note that the thrust and torque from a propeller are usually modeled as functions of the advance ratio alone. Wind-tunnel experimental data like the one documented in Fig. 13 show that this relationship might be too simplistic. Figure 13 shows the power and thrust coefficients of a small propeller that is used on hand-launched UAVs measured at three different propeller speed settings. At every setting, the advance ratio is varied by changing the wind-tunnel speed while keeping the propeller speed constant. The data show that C_P and C_T are not only functions of advance ratio but also rotational speed. In practice,

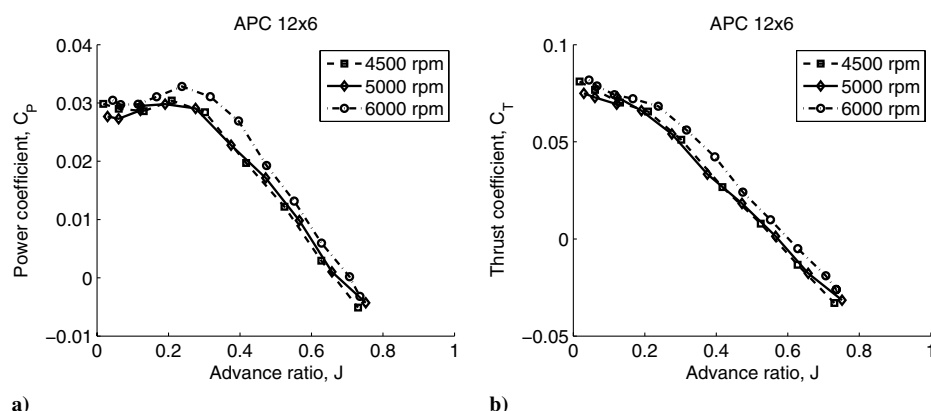


Fig. 13 APC 12 × 6 characteristics: a) power coefficient and b) thrust coefficient.

however, the functional relationship with the propeller speed is often neglected. When not neglected, propeller speed is measured using a tachometer that is going to be corrupted by random noise. Thus, the effects of the modeling errors are themselves stochastic. A complete stochastic analysis of the effect of such modeling errors on the estimation quality is beyond the scope of this paper.

VII. Conclusions

This paper presented a method for the synthetic estimation of airspeed, angle of attack, and sideslip. The estimator shows good performance on both simulated flight data and real flight data. The results of the flight-test data on the Ultrastick 120 show that the air data estimates compare very well against the conventional air data sensors on board. Moreover, the filter appears to be insensitive to modeling error, as shown in the good performance of the filter, despite using linearized equations of motion.

It is judged that the method such as the one presented in this paper will be indispensable in applications such as small UAVs or general aviation aircrafts, in which the luxury of having a multiple-air-data system is often unaffordable. In these instances, an approach like the one discussed in this paper can be used to provide analytical redundancy in addition to a traditional air data system or to serve as a backup to an existing traditional air data system.

Acknowledgments

The authors would like to thank Chandra Tjhai for sharing his experiment on propeller performance analysis. We gratefully acknowledge the help of Austin Murch, Arion Mangio, and the entire staff of the University of Minnesota's UAV Laboratory that has made flight testings possible.

Appendix A: Aerodynamic Force and Moment Model

$$C_T = C_{T_0} + C_{T_1}J + C_{T_2}J^2 + C_{T_3}J^3 \quad (\text{A1a})$$

$$C_P = C_{P_0} + C_{P_1}J + C_{P_2}J^2 + C_{P_3}J^3 + \dots + C_{P_9}J^9 \quad (\text{A1b})$$

$$C_D = C_{D_0} + C_{D_\beta}|\beta| + C_{D_a}\alpha + C_{D_a^2}\alpha^2 + C_{D_a^3}\alpha^3 + C_{D_a^4}\alpha^4 \quad (\text{A1c})$$

$$C_Y = C_{Y_\beta}\beta + C_{Y_p}\frac{pb}{2V} + C_{Y_r}\frac{rb}{2V} + C_{Y_{\delta_r}}\delta_r \quad (\text{A1d})$$

$$C_L = C_{L_0} + C_{L_a}\alpha + C_{L_a^2}\alpha^2 + C_{L_q}\frac{q\bar{c}}{2V} + C_{L_{\dot{\alpha}}}\frac{\dot{\alpha}\bar{c}}{2V} + C_{L_{\delta_e}}\delta_e \quad (\text{A1e})$$

$$C_l = C_{l_\beta}\beta + C_{l_p}\frac{pb}{2V} + C_{l_r}\frac{rb}{2V} + C_{l_{\delta_r}}\delta_r + C_{l_{\delta_a}}\delta_a \quad (\text{A2a})$$

$$C_m = C_{m_0} + C_{m_a}\alpha + C_{m_q}\frac{q\bar{c}}{2V} + C_{m_{\dot{\alpha}}}\dot{\alpha} + C_{m_{\delta_e}}\delta_e \quad (\text{A2b})$$

Table A1 Simulated Cessna 172 aerodynamic parameters

Property	Value
C_{T_0}	0.0677
C_{T_1}	0.0048
C_{T_2}	-0.0204
C_{T_3}	-0.0342
C_{P_0}	0.0571
C_{P_1}	0.2080
C_{P_2}	-1.8704
C_{P_3}	6.3336
C_{P_4}	-11.1477
C_{P_5}	10.9467
C_{P_6}	-6.1841
C_{P_7}	1.9859
C_{P_8}	-0.3339
C_{P_9}	0.0225
C_{D_0}	0.0340
C_{D_a}	0.1773
$C_{D_a^2}$	2.1112
$C_{D_a^3}$	7.7797
$C_{D_a^4}$	-36.2741
C_{D_β}	0.1700
C_{Y_β}	-0.3926
C_{Y_p}	-0.1450
C_{Y_r}	0.2670
$C_{Y_{\delta_r}}$	0.1870
C_{L_0}	0.2493
C_{L_a}	6.3434
$C_{L_a^2}$	-7.0820
C_{L_q}	3.9000
$C_{L_{\dot{\alpha}}}$	1.7000
$C_{L_{\delta_e}}$	0.4300
C_{l_β}	-0.0923
C_{l_p}	-0.4840
C_{l_r}	0.1869
$C_{l_{\delta_r}}$	0.0147
$C_{l_{\delta_a}}$	0.2290
C_{m_0}	0.1000
C_{m_a}	-1.8000
C_{m_q}	-12.4000
$C_{m_{\dot{\alpha}}}$	-7.2700
$C_{m_{\delta_e}}$	-1.1220
C_{n_β}	0.0587
C_{n_p}	-0.0278
C_{n_r}	-0.0937
$C_{n_{\delta_r}}$	-0.0430
$C_{n_{\delta_a}}$	-0.0053

Table A2 Physical and geometric properties of simulated Cessna 172

Property	Units	Value
Mass, m	kg	881.4598
Wingspan, b	m	10.9118
Wing area, S	m^2	16.1651
Mean aerodynamic chord, \bar{c}	m	1.4935
Moment of inertia, I_{xx}	$\text{kg} \cdot \text{m}^2$	1285.3154
Moment of inertia, I_{yy}	$\text{kg} \cdot \text{m}^2$	1824.9310
Moment of inertia, I_{zz}	$\text{kg} \cdot \text{m}^2$	2666.8939
Propeller coordinate, r_x	m	0.9576
Propeller coordinate, r_y	m	0.0000
Propeller coordinate, r_z	m	-0.6756

$$C_n = C_{n_\beta}\beta + C_{n_p}\frac{pb}{2V} + C_{n_r}\frac{rb}{2V} + C_{n_{\delta_r}}\delta_r + C_{n_{\delta_a}}\delta_a \quad (\text{A2c})$$

The following are the geometry and aerodynamic properties of a Cessna 172 model in JSBSim[¶]:

[¶]Data available online at http://wiki.flightgear.org/Cessna_172P [retrieved 13 March 2013].

Appendix B: Jacobian Matrix and Noise-Shaping Matrix Entries for State Covariance Propagation

Jacobian matrix, F :

$$F = \frac{\partial \mathcal{F}}{\partial \mathbf{x}} = \begin{bmatrix} F_{11} & F_{12} & F_{13} & 0_{3 \times 6} \\ F_{21} & F_{22} & 0_{3 \times 3} & 0_{3 \times 6} \\ 0_{3 \times 3} & F_{32} & F_{33} & 0_{3 \times 6} \\ 0_{6 \times 3} & 0_{6 \times 3} & 0_{6 \times 3} & F_{44} \end{bmatrix}$$

where

$$\begin{aligned} F_{11} &= \frac{1}{m} \begin{bmatrix} \frac{\partial X}{\partial u} & \frac{\partial X}{\partial v} & \frac{\partial X}{\partial w} \\ \frac{\partial Y}{\partial u} & 0 & 0 \\ \frac{\partial Z}{\partial u} & 0 & \frac{\partial Z}{\partial w} \end{bmatrix} & F_{12} &= \frac{1}{m} \begin{bmatrix} 0 & 0 & 0 \\ \frac{\partial Y}{\partial p} & 0 & \frac{\partial Y}{\partial r} \\ 0 & \frac{\partial Z}{\partial q} & 0 \end{bmatrix} & F_{13} &= \frac{1}{m} \begin{bmatrix} 0 & \frac{\partial X}{\partial \theta} & 0 \\ \frac{\partial Y}{\partial \phi} & \frac{\partial Y}{\partial \theta} & 0 \\ \frac{\partial Z}{\partial \phi} & \frac{\partial Z}{\partial \theta} & 0 \end{bmatrix} \\ F_{21} &= \begin{bmatrix} I_{xx} & 0 & I_{xz} \\ 0 & I_{yy} & 0 \\ I_{xz} & 0 & I_{yy} \end{bmatrix}^{-1} \begin{bmatrix} \frac{\partial \mathcal{L}}{\partial u} & \frac{\partial \mathcal{L}}{\partial v} & 0 \\ \frac{\partial \mathcal{M}}{\partial u} & 0 & \frac{\partial \mathcal{M}}{\partial w} \\ \frac{\partial \mathcal{N}}{\partial u} & \frac{\partial \mathcal{N}}{\partial v} & 0 \end{bmatrix} & F_{22} &= \begin{bmatrix} I_{xx} & 0 & I_{xz} \\ 0 & I_{yy} & 0 \\ I_{xz} & 0 & I_{yy} \end{bmatrix}^{-1} \begin{bmatrix} \frac{\partial \mathcal{L}}{\partial p} & 0 & \frac{\partial \mathcal{L}}{\partial r} \\ 0 & \frac{\partial \mathcal{M}}{\partial q} & 0 \\ \frac{\partial \mathcal{N}}{\partial p} & 0 & \frac{\partial \mathcal{N}}{\partial r} \end{bmatrix} & F_{32} &= \begin{bmatrix} 1 & \sin \phi \tan \theta & \cos \phi \tan \theta \\ 0 & \cos \phi & -\sin \phi \\ 0 & \sin \phi \sec \theta & \cos \phi \sec \theta \end{bmatrix} \\ F_{33} &= \begin{bmatrix} q \cos \phi \tan \theta - r \sin \phi \tan \theta & q \sin \phi \sec^2 \theta + r \cos \phi \sec^2 \theta & 0 \\ -q \sin \phi - r \cos \phi & 0 & 0 \\ q \cos \phi \sec \theta - r \sin \phi \sec \theta & q \cos \phi \sec \theta - r \sin \phi \sec \theta & 0 \end{bmatrix} & F_{44} &= \begin{bmatrix} -\frac{1}{\tau_{w_N}} & 0 & 0 & 0 & 0 & 0 \\ 0 & -\frac{1}{\tau_{w_E}} & 0 & 0 & 0 & 0 \\ 0 & 0 & -\frac{1}{\tau_{b_D}} & 0 & 0 & 0 \\ 0 & 0 & 0 & -\frac{1}{\tau_{b_\phi}} & 0 & 0 \\ 0 & 0 & 0 & 0 & -\frac{1}{\tau_{b_\theta}} & 0 \\ 0 & 0 & 0 & 0 & 0 & -\frac{1}{\tau_{b_y}} \end{bmatrix} \end{aligned}$$

Shaping matrix, G :

$$G = \begin{bmatrix} \mathcal{G} & 0_{6 \times 6} \\ 0_{3 \times 4} & 0_{3 \times 6} \\ 0_{6 \times 4} & \mathbf{I}_{6 \times 6} \end{bmatrix}, \quad \text{where } \mathcal{G} = \begin{bmatrix} 0 & 0 & 0 & \frac{1}{m} \frac{\partial X}{\partial \delta_f} \\ 0 & 0 & \frac{1}{m} \frac{\partial Y}{\partial \delta_r} & 0 \\ \frac{1}{m} \frac{\partial Z}{\partial \delta_e} & 0 & 0 & 0 \\ 0 & \frac{1}{I_{xx}} \frac{\partial \mathcal{L}}{\partial \delta_a} & \frac{1}{I_{xx}} \frac{\partial \mathcal{L}}{\partial \delta_r} & 0 \\ \frac{1}{I_{yy}} \frac{\partial \mathcal{M}}{\partial \delta_e} & 0 & 0 & 0 \\ 0 & \frac{1}{I_{zz}} \frac{\partial \mathcal{N}}{\partial \delta_a} & \frac{1}{I_{zz}} \frac{\partial \mathcal{N}}{\partial \delta_r} & 0 \end{bmatrix}$$

Aerodynamic derivatives:

$$\begin{aligned} \frac{\partial X}{\partial u} &= \frac{3C_{T_3}\rho u^2 d}{f} + 2C_{T_2}\rho ud^2 + \rho C_{T_0}fd^3 - \rho uSC_D + \frac{1}{2}\rho wSC_{D_a} & \frac{\partial X}{\partial v} &= \frac{1}{2}\rho uSC_{D_\beta} \operatorname{sgn}(v) & \frac{\partial X}{\partial w} &= \frac{1}{2}uSC_{D_a} + \rho wSC_{D_{\alpha^2}} \\ \frac{\partial X}{\partial \theta} &= -mg \cos \theta & \frac{\partial X}{\partial f} &= \rho uC_{T_1}d^3 & \frac{\partial Y}{\partial u} &= \rho uSC_Y - \frac{1}{2}\rho vSC_{Y_\beta} - \frac{1}{2}\rho SC_{Y_p} \frac{bp}{2} - \frac{1}{2}\rho SC_{Y_r} \frac{br}{2} & \frac{\partial Y}{\partial v} &= \frac{1}{2}\rho uSC_{Y_\beta} \\ \frac{\partial Y}{\partial p} &= \frac{1}{2}\rho u^2 SC_{Y_p} \left(\frac{b}{2u} \right) & \frac{\partial Y}{\partial r} &= \frac{1}{2}\rho u^2 SC_{Y_r} \left(\frac{b}{2u} \right) & \frac{\partial Y}{\partial \phi} &= -mg \sin \theta \sin \phi & \frac{\partial Y}{\partial \theta} &= mg \cos \theta \cos \phi & \frac{\partial Y}{\partial \delta_r} &= \frac{1}{2}\rho u^2 SC_{Y_r} \\ \frac{\partial Z}{\partial u} &= -\rho uSC_L + \frac{1}{2}\rho wSC_{L_a} & \frac{\partial Z}{\partial w} &= -\frac{1}{2}\rho uSC_{L_a} - \rho wSC_{L_{a^2}} & \frac{\partial Z}{\partial q} &= -\frac{1}{2}\rho u^2 SC_{L_q} \left(\frac{\bar{c}}{2u} \right) & \frac{\partial Z}{\partial \delta_e} &= -\frac{1}{2}\rho u^2 SC_{L_{\delta_e}} \\ \frac{\partial Z}{\partial \phi} &= -mg \sin \theta \cos \phi & \frac{\partial Z}{\partial \theta} &= -mg \cos \theta \sin \phi & \frac{\partial \mathcal{L}}{\partial u} &= \rho uSbC_l & \frac{\partial \mathcal{L}}{\partial v} &= \frac{1}{2}\rho uSbC_{l_\beta} \\ \frac{\partial \mathcal{L}}{\partial p} &= \frac{1}{2}\rho u^2 SbC_{l_p} \left(\frac{b}{2u} \right) & \frac{\partial \mathcal{L}}{\partial r} &= \frac{1}{2}\rho u^2 SbC_{l_r} \left(\frac{b}{2u} \right) & \frac{\partial \mathcal{L}}{\partial \delta_a} &= \frac{1}{2}\rho u^2 SbC_{n_r} \left(\frac{b}{2u} \right) & \frac{\partial \mathcal{L}}{\partial \delta_r} &= \frac{1}{2}\rho u^2 SbC_{n_r} \left(\frac{b}{2u} \right) & \frac{\partial \mathcal{M}}{\partial u} &= \rho uS\bar{c}C_m \\ \frac{\partial \mathcal{M}}{\partial w} &= \frac{1}{2}\rho uSC\bar{c}C_{m_\beta} & \frac{\partial \mathcal{M}}{\partial q} &= \frac{1}{2}\rho u^2 S\bar{c}C_{m_q} \left(\frac{\bar{c}}{2u} \right) & \frac{\partial \mathcal{M}}{\partial \delta_e} &= \frac{1}{2}\rho u^2 S\bar{c}C_{m_{\delta_e}} \left(\frac{\bar{c}}{2u} \right) & \frac{\partial \mathcal{N}}{\partial u} &= \rho uSbC_n & \frac{\partial \mathcal{N}}{\partial v} &= \frac{1}{2}\rho uSbC_{n_\beta} \\ \frac{\partial \mathcal{N}}{\partial p} &= \frac{1}{2}\rho u^2 SbC_{n_p} \left(\frac{b}{2u} \right) & \frac{\partial \mathcal{N}}{\partial r} &= \frac{1}{2}\rho u^2 SbC_{n_r} \left(\frac{b}{2u} \right) & \frac{\partial \mathcal{N}}{\partial \delta_a} &= \frac{1}{2}\rho u^2 SbC_{n_r} \left(\frac{b}{2u} \right) & \frac{\partial \mathcal{N}}{\partial \delta_r} &= \frac{1}{2}\rho u^2 SbC_{n_r} \left(\frac{b}{2u} \right) \end{aligned}$$

Table C1 Stability derivatives^a

Parameter	Units	Value	Parameter	Units	Value	Parameter	Units	Value
X_u	(m/s) ⁻¹	-0.4082	M_u	(m/s) ⁻¹	0.3423	L_v	(m/s) ⁻¹	-1.7060
X_w	(m/s) ⁻¹	0.7003	M_w	(m/s) ⁻¹	-1.9350	L_p	(rad/s) ⁻¹	-10.7800
X_q	(rad/s) ⁻¹	-1.7100	M_q	(rad/s) ⁻¹	-9.0690	L_r	(rad/s) ⁻¹	2.2070
X_θ	rad ⁻¹	-9.7850	M_{δ_e}	rad ⁻¹	-104.0000	L_{δ_a}	rad ⁻¹	-134.1000
X_{δ_e}	rad ⁻¹	1.0340	Y_v	(m/s) ⁻¹	-0.5943	L_{δ_r}	rad ⁻¹	2.3640
Z_u	(m/s) ⁻¹	-0.2599	Y_p	(rad/s) ⁻¹	1.6600	N_v	(m/s) ⁻¹	0.8312
Z_w	(m/s) ⁻¹	-7.4240	Y_r	(rad/s) ⁻¹	-25.9700	N_p	(rad/s) ⁻¹	0.8274
Z_q	(rad/s) ⁻¹	26.4400	Y_ϕ	rad ⁻¹	9.7850	N_r	(rad/s) ⁻¹	-1.8860
Z_θ	rad ⁻¹	-0.6329	Y_{δ_a}	rad ⁻¹	0	N_{δ_a}	rad ⁻¹	14.9700
Z_{δ_e}	rad ⁻¹	-13.2200	Y_{δ_r}	rad ⁻¹	0.3862	N_{δ_r}	rad ⁻¹	-10.6700

^aTrim condition: steady-level flight at $V = 26.5$ m/s.

Table C2 Physical and geometric properties of Ultrastick 120

Property	Units	Value
Mass, m	kg	7.4110
Wingspan and area; b, S	m, m ²	1.9172, 0.7692
Mean aerodynamic chord, \bar{c}	m	0.4336
Moment of inertia, I_{xx}	kg · m ²	0.8568
Moment of inertia, I_{yy}	kg · m ²	1.0095
Moment of inertia, I_{zz}	kg · m ²	1.7005
Moment of inertia, I_{xz}	kg · m ²	-0.1898
Propeller coordinates, $[r_x, r_y, r_z]$	m	[-0.0750, 0, 0]

Appendix C: Ultrastick 120 Linear Model

Longitudinal mode:

$$\dot{\mathbf{x}}_{\text{lon}} = \mathbf{A}_{\text{lon}} \mathbf{x}_{\text{lon}} + \mathbf{B}_{\text{lon}} \mathbf{u}_{\text{lon}} \quad \mathbf{x}_{\text{lon}} = [u \quad w \quad q \quad \theta]^T$$

$$\mathbf{u}_{\text{lon}} = \delta_e \quad \mathbf{A}_{\text{lon}} = \begin{bmatrix} X_u & X_w & X_q & X_\theta \\ Z_u & Z_w & Z_q & Z_\theta \\ M_u & M_w & M_q & 0 \\ 0 & 0 & 1 & 0 \end{bmatrix} \quad \mathbf{B}_{\text{lon}} = \begin{bmatrix} X_{\delta_e} \\ Z_{\delta_e} \\ M_{\delta_e} \\ 0 \end{bmatrix}$$

Lateral-directional mode:

$$\dot{\mathbf{x}}_{\text{lat}} = \mathbf{A}_{\text{lat}} \mathbf{x}_{\text{lat}} + \mathbf{B}_{\text{lat}} \mathbf{u}_{\text{lat}} \quad \mathbf{x}_{\text{lat}} = [v \quad p \quad r \quad \phi \quad \psi]^T$$

$$\mathbf{u}_{\text{lat}} = [\delta_a \quad \delta_r]^T \quad \mathbf{A}_{\text{lat}} = \begin{bmatrix} Y_v & Y_p & Y_r & Y_\phi & 0 \\ L_v & L_p & L_r & 0 & 0 \\ N_v & N_p & N_r & 0 & 0 \\ 0 & 1 & 0 & 0 & 0 \\ 0 & 0 & 1 & 0 & 0 \end{bmatrix}$$

$$\mathbf{B}_{\text{lat}} = \begin{bmatrix} Y_{\delta_a} & Y_{\delta_r} \\ L_{\delta_a} & L_{\delta_r} \\ N_{\delta_a} & N_{\delta_r} \\ 0 & 0 \\ 0 & 0 \end{bmatrix}$$

Trim condition:

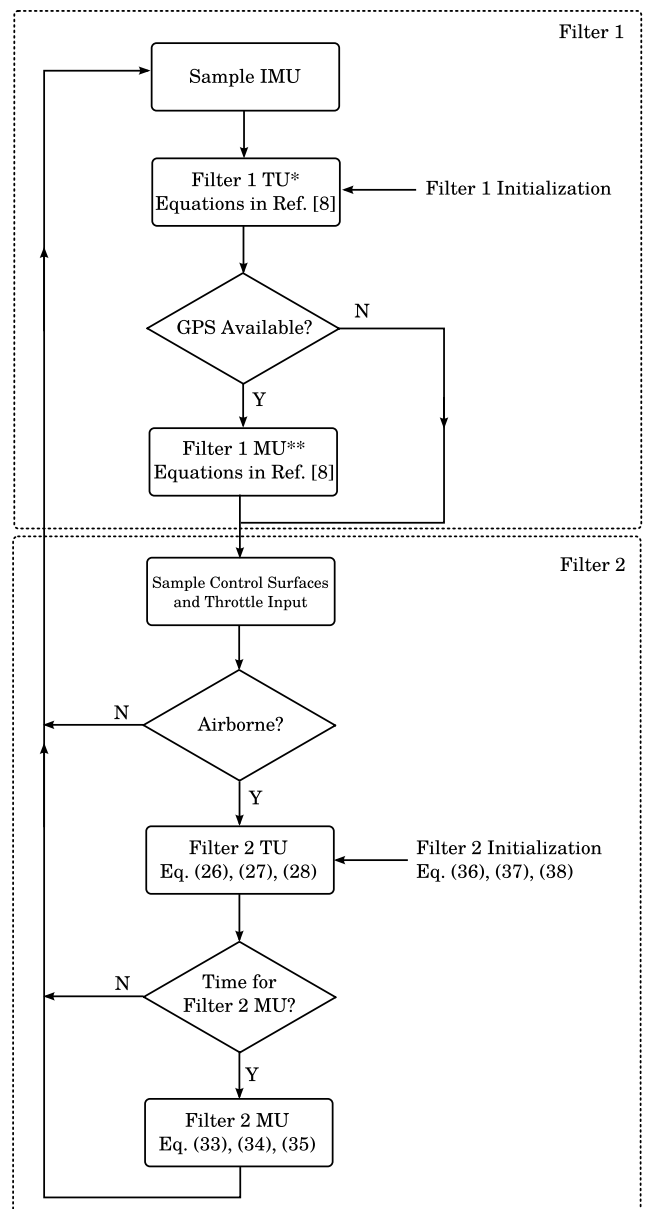
$$u = 26.5 \cos(0.0646 \text{ rad}) \text{ m/s} \quad p = q = r = 0 \text{ rad/s}$$

$$\delta_e = -0.0646 \text{ rad} \quad v = 0 \text{ m/s} \quad \phi = 0 \text{ rad}$$

$$\delta_a = -0.0051 \text{ rad} \quad w = 26.5 \sin(0.0646 \text{ rad}) \text{ m/s}$$

$$\theta = 0.0646 \text{ rad} \quad \delta_r = 0 \text{ rad}$$

Appendix D: Synthetic Air Data Estimator Flow Chart



* TU : Time Update

**MU : Measurement Update

Fig. D1 Synthetic air data estimator flow chart.

References

- [1] Spoerry, T., and Chauveau, B., U.S. Patent Application for "Device and Method for Estimating a Sideslip Angle of an Aircraft," Docket No. 7,835,884 B2, filed 16 Nov. 2010.
- [2] Wheeler, T. J., Seiler, P., Packard, A. K., and Balas, G. J., "Performance Analysis of Fault Detection System Based on Analytically Redundant Linear Time-Invariant Dynamics," *Proceedings of American Control Conference (ACC)*, San Francisco, June 2011, pp. 214–249.
- [3] Zeis, J. E., "Angle-of-Attack and Sideslip Estimation Using Inertial Reference Platform," M.S. Thesis, School of Engineering, Air Force Inst. of Technology, Wright-Patterson AFB, OH, 1988.
- [4] Heller, M., Myschik, S., Holzapfel, F., and Sachs, G., "Low-Cost Approach Based on Navigation Data for Determining Angles of Attack and Sideslip for Small Aircraft," *Proceedings of AIAA Guidance, Navigation, and Control Conference and Exhibit*, AIAA Paper 2003-5777, Austin, TX, Aug. 2003.
- [5] Myschik, S., Holzapfel, F., and Sachs, G., "Low-Cost Sensor Based Integrated Airdata and Navigation System for General Aviation Aircraft," *Proceedings of AIAA Guidance, Navigation, and Control Conference and Exhibit*, AIAA Paper 2008-7423, Honolulu, HI, Aug. 2008.
- [6] Murch, A., "A Flight Control System Architecture for the NASA AirSTAR Flight Test Infrastructure," *Proceedings of AIAA Guidance, Navigation, and Control Conference and Exhibit*, AIAA Paper 2008-6990, Honolulu, HI, Aug. 2008.
- [7] Groves, P. D., *Principles of GNSS, Inertial, and Integrated Navigation Systems*, Artech House, Norwood, MA, 2008.
- [8] Gleason, S., and Gebre-Egziabher, D., *GNSS Applications and Methods*, Artech House, Norwood, MA, 2009.
- [9] Colgren, R. D., "The Feasibility of Using an INS for Control System Feedbacks," *1998 World Aviation Congress*, Aug. 1998.
- [10] Colgren, R. D., Frye, M. T., and Olson, W. M., "A Proposed System Architecture for Estimation of Angle of Attack and Sideslip Angle," *Proceedings of AIAA Guidance, Navigation, and Control Conference and Exhibit*, AIAA Paper 1999-4078, Portland, OR, Aug. 1999.
- [11] Colgren, R. D., and Martin, K. E., "Flight Test Validation of Sideslip Estimation Using Inertial Accelerations," *Proceedings of AIAA Guidance, Navigation, and Control Conference and Exhibit*, AIAA Paper 2000-4448, Denver, CO, Aug. 2000.
- [12] Colgren, R. D., U.S. Patent Application for "Method and System for Elimination and Correction of Angle of Attack and Sideslip Angle from Acceleration Measurements," Docket No. 6,273,370, filed 14 Aug. 2001.
- [13] Wise, K. A., "Flight Testing of the X-45A J-UCAS Computational Alpha-Beta System," *Proceedings of AIAA Guidance, Navigation, and Control Conference and Exhibit*, AIAA Paper 2006-6215, Keystone, CO, Aug. 2006.
- [14] Wise, K. A., U.S. Patent Application for "Computational Air Data System Using Angle-of-Attack and Angle-of-Sideslip," Docket No. 6,928,341, 9, filed Aug. 2005.
- [15] Langelaan, J. W., Alley, N., and Neidhofer, J., "Wind Field Estimation for Small Unmanned Aerial Vehicles," *Journal of Guidance, Control, and Dynamics*, Vol. 34, No. 4, 2011, pp. 1016–1030.
doi:10.2514/1.52532
- [16] Cho, A., Kim, J., Lee, S., and Kee, C., "Wind Estimation and Airspeed Calibration Using the UAV with a Single-Antenna GNSS Receiver and Airspeed Sensor," *Proceedings of the 19th International Technical Meeting of the Satellite Division of The Institute of Navigation (ION GNSS 2006)*, Fort Worth, TX, 2006, pp. 3050–3058.
- [17] Foster, J. V., and Cunningham, K., "A GPS-Based Pitot-Static Calibration Method Using Global Output-Error Optimization," *Proceedings of 48th AIAA Aerospace Sciences Meeting Including the New Horizons Forum and Aerospace Exposition*, AIAA Paper 2010-1350, Orlando, FL, Jan. 2010.
- [18] Lie, F. A. P., and Gebre-Egziabher, D., "A Synthetic Airdata Estimator," *Proceedings of AIAA Guidance, Navigation, and Control Conference and Exhibit*, AIAA Paper 2012-4704, Minneapolis, MN, Aug. 2012.
- [19] Hemesath, N. B., "Optimum Complementation of VOR/DME with Air Data," *Journal of Aircraft*, Vol. 8, No. 6, 1971, pp. 456–460.
doi:10.2514/3.59123
- [20] Bryson, A. E., and Bobick, J. C., "Improved Navigation by Combining VOR/DME Information and Air Data," *Journal of Aircraft*, Vol. 9, No. 6, 1972, pp. 420–426.
doi:10.2514/3.59006
- [21] Berman, Z., and Powell, J. D., "The Role of Dead Reckoning and Inertial Sensors in Future General Aviation Navigation," *IEEE Position Location and Navigation Symposium*, Palm Springs, CA, 1998, pp. 510–517.
- [22] Boeing Co., *737 Flight Crew Operations Manual*, 2006.
- [23] Simon, D., "Kalman Filtering with State Constraints: A Survey of Linear and Nonlinear Algorithms," *IET Control Theory and Applications*, Vol. 4, No. 8, Aug. 2010, pp. 1303–1318.
doi:10.1049/iet-cta.2009.0032
- [24] Bevly, D. M., and Parkinson, B., "Cascaded Kalman Filters for Accurate Estimation of Multiple Biases, Dead-Reckoning Navigation, and Full State Feedback Control of Ground Vehicles," *IEEE Transactions on Control Systems Technology*, Vol. 15, No. 2, 2007, pp. 199–208.
doi:10.1109/TCST.2006.883311
- [25] Friedland, B., "Treatment of Bias in Recursive Filtering," *IEEE Transactions on Automatic Control*, Vol. 14, No. 4, 1969, pp. 359–367.
doi:10.1109/TAC.1969.1099223
- [26] Alouani, A. T., Xia, P., Rice, T. R., and Blair, W. D., "On the Optimality of Two-Stage State Estimation in the Presence of Random Bias," *IEEE Transactions on Automatic Control*, Vol. 38, No. 8, Aug. 1993, pp. 1279–1282.
doi:10.1109/9.233168
- [27] Haupt, G. T., Kasdin, N. J., Kaiser, G. M., and Parkinson, B. W., "Optimal Recursive Iterative Algorithm for Discrete Nonlinear Least-Squares Estimation," *Journal of Guidance, Control, and Dynamics*, Vol. 19, No. 3, 1996, pp. 643–649.
doi:10.2514/3.21669
- [28] Titterton, D. H., and Weston, J. L., *Strapdown Inertial Navigation Technology*, Institution of Engineering and Technology, Stevenage, England, U.K., 2004.
- [29] Farrell, J., and Barth, M., *The Global Positioning System and Inertial Navigation*, McGraw-Hill, New York, 1999.
- [30] Etkin, B., "General Equations of Unsteady Motion," *Dynamics of Atmospheric Flight*, Dover, Mineola, NY, 2000, pp. 121–195.
- [31] Stengel, R. F., *Optimal Control and Estimation*, Dover, New York, 1994.
- [32] Simon, D., "Kalman Filter Generalizations," *Optimal State Estimation: Kalman, H_{∞} , and Nonlinear Approaches*, Wiley, Hoboken, NJ, 2006, pp. 188–193.
- [33] Xing, Z., "Over-Bounding Integrated INS/GNSS Output Errors," Ph.D. Dissertation, Dept. of Aerospace Engineering and Mechanics, Univ. of Minnesota, Minneapolis, MN, 2010.
- [34] Franklin, G. F., Powell, J. D., and Workman, M. L., *Digital Control of Dynamic Systems*, Addison Wesley Longman, Reading, MA, 1998.
- [35] Owens, D. B., Cox, D. E., and Morelli, E. A., "Development of a Low-Cost SubScale Aircraft for Flight Research: The FASER Project," *Proceedings of 25th AIAA Aerodynamic Measurement Technology and Ground Testing Conference*, AIAA Paper 2006-3306, San Francisco, 2006.
- [36] Kershner, D. D., "Miniature Flow-Direction and Airspeed Sensor for Airplanes and Radio-Controlled Models in Spin Studies," NASA TP-1467, May 1979.